NASA
Technical
Paper
2758

September 1987

Application of Turbulence Modeling to Predict Surface Heat Transfer in Stagnation Flow Region of Circular Cylinder

Chi R. Wang and
Frederick C. Yeh

NASA

NASA Technical Paper 2758

1987

Application of Turbulence Modeling to Predict Surface Heat Transfer in Stagnation Flow Region of Circular Cylinder

Chi R. Wang and
Frederick C. Yeh

Lewis Research Center
Cleveland, Ohio

National Aeronautics
and Space Administration

**Scientific and Technical
Information Office**

Summary

A theoretical analysis and numerical calculations for the turbulent flow field and for the effect of free-stream turbulence on the surface heat transfer rate of a stagnation flow are presented. The flow field considered is the region near the forward stagnation point of a circular cylinder in a uniform turbulent mean flow. The emphasis of the present study is on the modeling of turbulence and its augmentation of the surface heat transfer rate. The free stream is steady and incompressible with a Reynolds number of the order of 10^5 and a turbulence intensity of less than 5 percent. In the analysis, the flow field is divided into three regions: (1) a region significantly away from the cylinder where the mean velocity is uniform and the turbulence is homogeneous and isotropic, (2) an external inviscid flow region with a constant rate of the mean velocity variation where the turbulence is distorted by the mean flow velocity, and (3) an anisotropic turbulent boundary layer region over the cylinder surface. The turbulence modeling techniques used are the k–ϵ two-equation model in the external flow region and the time-averaged turbulence transport equation in the boundary layer region. The turbulence double correlations, the mean velocity, and the mean temperature are solved numerically from sets of finite difference equations. These finite difference equations are derived from the flow-field governing equations. The solution is obtained from matching the turbulence kinetic energy along the boundaries between the flow regions. The results and their comparisons with the experiments show that (1) depending on the free-stream turbulence characteristics, the turbulence kinetic energy is amplified or attenuated along the stagnation-point streamline, (2) the free-stream turbulence penetrates into the flow region near the surface and induces a high surface heat transfer rate, (3) the turbulence kinetic energy increases continuously in the mean flow direction along the boundary layer edge and, near the stagnation point, the rate of variation in the Reynolds normal stress is different for each component, (4) depending on the level of the turbulence kinetic energy, different surface heat transfer rates may occur near the stagnation point, and (5) the analysis provides a procedure in computing the surface heat transfer rate near a stagnation point as functions of the turbulence longitudinal microlength scale, the turbulence intensity, and the free-stream Reynolds number.

Introduction

The momentum and thermal flow fields near the forward stagnation point of a circular cylinder in turbulent flow have been the focus of considerable study (refs. 1 to 12). One objective has been to understand the enhancement of the heat transfer due to the free-stream turbulence near the leading edge of an airfoil. Existing experiments (refs. 3 and 4) have shown that when the turbulence intensity is 3 to 5 percent the local Nusselt number increases by 75 percent as compared with laminar flow conditions. In the initial stage of turbine blade design, the blade leading edge is often modeled as a circular cylinder in a turbulent free stream. With the current emphasis on high turbine inlet temperature, it has become even more important to understand the effect of turbulence on the surface heat transfer, particularly at the leading-edge stagnation region. In fact, prediction of the stagnation-region surface heat transfer becomes vital to the turbine blade cooling design. To estimate this surface heat transfer rate, correlations derived from experimental data may be used. Detailed experimental data can be found in the paper by Lowery and Vachon (ref. 5). The alternative is to rely on the analysis to obtain the surface heat transfer rate. The objective of the present study is to develop an analytical method that can predict the effect of the turbulence on the surface heat transfer rate.

Smith and Kuethe (ref. 6) used the two-dimensional boundary layer theory to analyze the flow at the stagnation point on a circular cylinder. The eddy viscosity was assumed to be proportional to the turbulence in the free stream. Reynolds' analogy was used. This analysis indicates a large effect of turbulence on heat transfer. A similar analytical approach was used by Gorla (ref. 7) to investigate the effects of the unsteadiness in the free stream and its turbulence on heat transfer at a stagnation point. Other studies (refs. 8 to 11) show that turbulence amplification, because of vortex stretching, can also influence the thin boundary layer and, therefore, the surface heat transfer rate.

To model the turbulence effect, Hijikata et al. (ref. 12) performed a theoretical and experimental study of the stagnation-point anisotropic turbulence. An equation for the anisotropic turbulence was added to the k–ϵ two-equation turbulence modeling to analyze the measurements. Their analysis shows that the turbulence length scale affects the

surface heat transfer rate. Traci and Wilcox (ref. 13) analytically studied the turbulence effect on the stagnation-point flow field using Saffman turbulence modeling (ref. 14). The mean velocity gradients within the inviscid flow were found to be important in analyzing the stagnation-point heat transfer. A difficulty in this type of analysis is attaining a proper match of the boundary conditions between the different flow regions. Strahle (ref. 15) tried to resolve analytically the turbulence matching conditions. Analytical relations between the turbulence kinetic energy and its dissipation rate at the stagnation point and in the free stream were found. On the basis of the method of invariant modeling (refs. 16 and 17), Wang (ref. 18) proposed a theoretical boundary layer flow analysis and numerical computational procedure to investigate the turbulence, momentum, and thermal fields within the stagnation flow region. Ad hoc turbulence boundary conditions were imposed along the boundary layer edge. The numerical calculation showed that rapid amplification of the Reynolds normal stresses along the boundary layer edge was required to predict the approximate surface heat transfer rate as reported in existing experiments.

From the experimental results and analytical methods of these existing studies, it is possible to pursue a detailed theoretical and numerical analysis of the forward stagnation flow field of a circular cylinder in a turbulent free stream. Reported herein is such an analysis, which provides a procedure to compute the surface heat transfer rate as functions of the free-stream turbulence longitudinal microlength scale, the turbulence intensity, and the Reynolds number. The emphasis is on the modeling of turbulence and its augmentation of the surface heat transfer rate.

The stagnation flow field is divided into three distinct regions: (1) a region away from the cylinder where the mean velocity is uniform and the turbulence is assumed to be homogeneous and isotropic, (2) an external inviscid flow region which has a constant rate of mean velocity variation and the mean velocity distorts the turbulence, and (3) an anisotropic turbulent boundary layer region over the cylinder surface. For turbulence modeling, the k–ϵ two-equation modeling and the time-averaged turbulence transport equation are used respectively in flow regions 2 and 3. These turbulence modeling equations and the mean flow conservation equations are used to formulate the theoretical analysis. The turbulence double correlations, the mean velocity, and the mean temperature are solved numerically from sets of finite difference equations. The solution is obtained from matching the turbulence kinetic energy along the boundary between the flow regions. These analytical results are compared with the measurements from existing experiments.

Symbols

A_{Gi}	coefficients of equation (C1), $i = 1$ to 9
a	mean velocity parameter
B_i	coefficients of equation (C6), $i = 1$ to 4
c_i	empirical constants, $i = 1$ to 5
c_p	specific heat
c_μ	empirical constant
D	cylinder diameter
E	dimensionless turbulence dissipation rate
F	dimensionless mean flow streamwise velocity
f_i	parametrical functions of φ, $i = 1$ to 3
G	flow variable of equation (C1)
g	turbulence longitudinal correlation
H	dimensionless mean temperature
K	dimensionless turbulence kinetic energy
k	turbulence kinetic energy
ℓ	spatial distance
Nu	Nusselt number
P	mean static pressure
Pr	laminar Prandtl number, 0.7
p	pressure fluctuation
R	sum of dimensionless Reynolds normal stresses, $R_x + R_y + R_z$
R_x	dimensionless Reynolds normal stress along x direction
R_y	dimensionless Reynolds normal stress along y direction
R_z	dimensionless Reynolds normal stress along z direction
Re	Reynolds number
S	dimensionless Reynolds shear stress
T	mean temperature
Tu	free-stream turbulence intensity, $\sqrt{\overline{v_F^2}}/V_F$
t	temperature fluctuation
U,V	mean velocity components
V_t	transformed velocity of V (eq. (13))
ν_t	turbulent dynamic viscosity
u,v,w	velocity fluctuations
x,y,z	physical coordinate system
δ	stagnation-point laminar boundary layer thickness
ϵ	turbulence dissipation rate
η	transformed coordinate along y direction
θ	dimensionless turbulence correlation, $-\overline{vt}/U_eT_e$
κ	thermal conductivity
Λ	turbulence modeling length scale
λ	turbulence longitudinal microlength scale
ν	kinematic viscosity
ξ	transformed coordinate along x direction
ρ	density
φ	azimuth angle

Subscripts:

e	external or boundary layer edge condition
F	free-stream condition
m	grid point along ξ or η direction
o,e	boundary layer edge condition at initial station
w	surface condition
0	condition near stagnation point
1	condition at location 1
2	condition at location 2 of boundary layer edge
3	condition at location 3 of boundary layer edge

Superscript:

—	time mean average

Analytical Formulation of Flow Regions

The flow region of interest is around the forward stagnation point of a circular cylinder in a turbulent free stream. Figure 1 schematically represents the flow field. The diameter of the cylinder is D and its axis is perpendicular to the free-stream mean velocity V_F. The free-stream Reynolds number is defined as $Re = V_F D/\nu$, where ν is the kinematic viscosity. The velocity fluctuation in the free stream is v_F, and the free-stream turbulence intensity is defined as $Tu = \sqrt{\overline{v_F^2}}/V_F$. The free-stream turbulence longitudinal microlength scale is denoted by λ_F. The cylinder is assumed to have a constant surface temperature T_w. The free-stream temperature is T_F.

The stagnation point is taken as the coordinate-system origin; x and y denote the distances parallel to and normal to the cylinder surface; and z denotes the distance parallel to the cylinder axis. The mean flow field is assumed to be steady, incompressible, and two dimensional. The mean velocity components are U and V along the x and y coordinates. The turbulence is three dimensional. The velocity fluctuations are denoted by $\overline{u^2}$, $\overline{v^2}$, and $\overline{w^2}$ along the x, y, and z directions. To formulate the theoretical analysis, the flow field is divided into three flow regions. The governing equations of the mean flow and the turbulence are derived for each flow region. Following the laminar flow analysis, the relations

$$\xi(x) = \int_0^x \frac{U_e}{\nu} dx \quad \text{and} \quad \eta(x,y) = \frac{\dfrac{U_e v}{\nu}}{(2\xi)^{0.5}} \tag{1}$$

are used for coordinate transformation. The analytical formulation, together with the assumptions and the boundary conditions, for each flow region is described here.

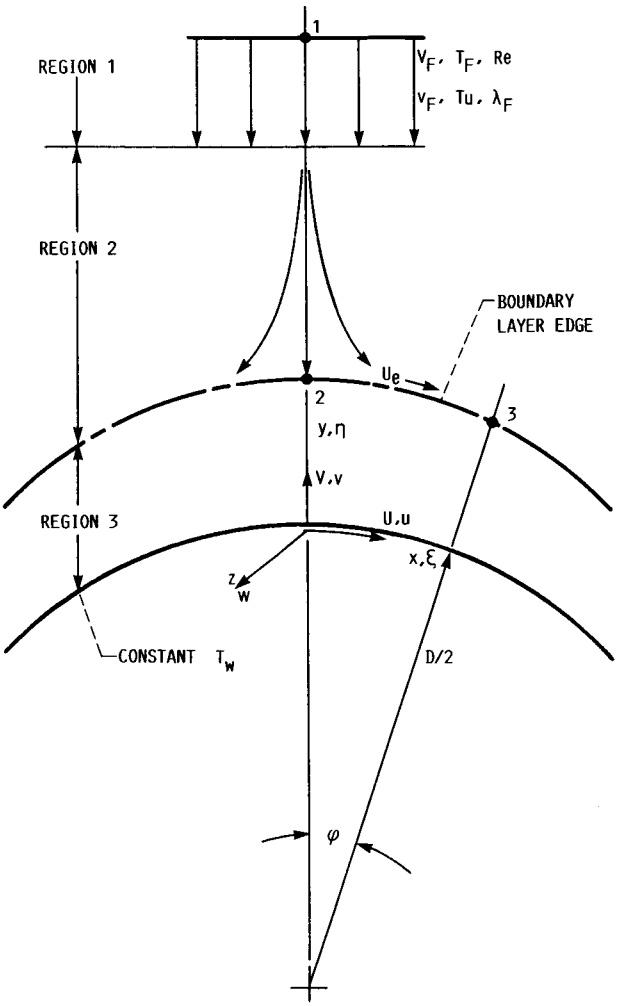

Figure 1.—Schematic of flow field of interest.

Region 1

This flow region is the uniform turbulent free stream away from the cylinder. The properties of the mean flow and the turbulence are not influenced by the existence of the cylinder. Appropriate conditions of the turbulence kinetic energy k and the turbulence dissipation rate ϵ are required to characterize the turbulence. The turbulence is assumed to be homogeneous and isotropic. The free-stream turbulence kinetic energy and the turbulence dissipation rate are given by the following equations (ref. 19):

$$k_F = \frac{3\overline{v_F^2}}{2} \quad \text{and} \quad \epsilon_F = \frac{30\nu\overline{v_F^2}}{\lambda_F^2} \tag{2}$$

The turbulence longitudinal microlength scale can be determined from the isotropic turbulence theory and two-point turbulence correlations. The two-point turbulence longitudinal correlation g, the spatial distance ℓ, and the free-stream turbulence longitudinal microlength scale λ_F are related by the following equation:

$$g(\ell) = 1 - \frac{\ell^2}{\lambda_F^2} \tag{3}$$

with small values of ℓ.

Region 2

In this region, the mean flow velocity is disturbed by the cylinder. The mean velocity variation distorts the turbulence. However, the turbulence does not influence the mean flow velocity. Thus, the mean flow is represented with the two-dimensional inviscid flow solution near the stagnation point. The mean flow velocity components are

$$U = ax \quad \text{and} \quad V = -ay \tag{4}$$

with $a = 4V_F/D$. The turbulence kinetic energy variation along the stagnation-point streamline is of interest in this study. The turbulence is modeled with the k–ϵ two-equation turbulence model. A summary of this modeling technique is given in appendix A. For convenience, the x direction diffusion terms are neglected in the k and ϵ equations. Along the stagnation-point streamline, the following forms of the k and ϵ equations are found:

$$ay\frac{dk}{dy} = -4a^2c_\mu\frac{k^2}{\epsilon} + \epsilon - \frac{d}{dy}\left(c_\mu\frac{k^2}{c_{3\epsilon}}\frac{dk}{dy}\right) \tag{5}$$

$$ay\frac{d\epsilon}{dy} = -4a^2c_1c_\mu k + c_2\frac{\epsilon^2}{k} - \frac{d}{dy}\left(c_\mu\frac{k^2}{c_{4\epsilon}}\frac{d\epsilon}{dy}\right) \tag{6}$$

Introducing the coordinate transformations (eq. (1)) and the following forms of solutions for k and ϵ,

$$k = \nu aK(\eta) \quad \text{and} \quad \epsilon = \nu a^2E(\eta) \tag{7}$$

results in the following k and ϵ equations:

$$\eta\frac{dK}{d\eta} = -4c_\mu\frac{K^2}{E} + E - \frac{d}{d\eta}\left(c_\mu\frac{K^2}{c_3E}\frac{dK}{d\eta}\right) \tag{8}$$

$$\eta\frac{dE}{d\eta} = -4c_1c_\mu K + c_2\frac{E^2}{K} - \frac{d}{d\eta}\left(c_\mu\frac{K^2}{c_4E}\frac{dE}{d\eta}\right) \tag{9}$$

Equations (8) and (9) are solved for the turbulence properties K and E in the interval $\eta_1 \geq \eta \geq \eta_2$ along the stagnation streamline, where η_1 is the boundary between flow regions 1 and 2 and η_2 is the boundary between flow regions 2 and 3.

The boundary conditions are defined in the following:
(1) At $\eta = \eta_1$,

$$K = K_1 = \frac{k_F}{\nu a} \quad \text{and} \quad E = E_1 = \frac{\epsilon_F}{\nu a^2} \tag{10}$$

where k_F and ϵ_F are previously determined by equation (2).

(2) By neglecting the diffusion term in equation (9) at η_1, this equation gives the following additional boundary condition at $\eta = \eta_1$:

$$\frac{dE}{d\eta} = \frac{1}{\eta_1}\left(c_2\frac{E_1^2}{K_1} - 4c_1c_\mu K_1\right) \tag{11}$$

(3) It is also further assumed (ref. 13) that

$$\frac{dK}{d\eta} = 0 \quad \text{at } \eta = \eta_2 \tag{12}$$

The finite difference method is used to solve the boundary value problem in equations (8) to (12). Appendix C contains a description of the numerical method. The relation $\eta_1 = V_F/(\nu a)^{0.5}$ is found from equations (1) and (4), and η_2 is resolved in the process of the numerical calculation.

The solutions of the turbulence properties in flow region 2, obtained in the manner described previously, provide the turbulence quantities K and E at $\eta = \eta_2$. These turbulence quantities are required for the analysis of the boundary layer flow region.

Region 3

A steady, two-dimensional, incompressible turbulent boundary layer flow is assumed in this near-wall region. The mean flow properties are described by the boundary layer continuity, momentum, and enthalpy equations. The momentum and enthalpy equations contain the turbulence double correlations $\overline{uv}$ and $\overline{vt}$. These double correlations are related to the higher order turbulence correlations and the mean flow properties through the transport of the turbulence. A method to model the turbulence double correlations was developed by Donaldson et al. (refs. 16 and 17). This method is used to formulate a theoretical analysis of the turbulence in this flow region. The Reynolds stress transport equations are derived by following the theory in reference 16. Assumptions are made for the turbulence closure relations and a modeling length scale Λ. A summary of the theoretical formulation and assumptions is given in appendix B.

For the present boundary layer flow analysis, the mean velocity, $U_e = ax$, is assumed along the boundary layer edge

between regions 2 and 3. The mean flow properties and turbulence double correlations are also nondimensionalized as

$$F = \frac{U}{U_e}, \qquad H = \frac{T}{T_e}$$

$$R_x = \frac{\overline{u^2}}{U_e^2}, \qquad R_y = \frac{\overline{v^2}}{U_e^2}, \qquad R_z = \frac{\overline{w^2}}{U_e^2}$$

$$S = -\frac{\overline{uv}}{U_e^2}, \qquad \theta = -\frac{\overline{vt}}{U_e T_e}$$

Introducing the previous dimensionless variables and the coordinate transformations (eq. (1)) into the mean flow and turbulence transport equations (see appendix B) results in the following forms of the flow-field governing equations:

Continuity equation:

$$2\xi\frac{\partial F}{\partial \xi} + \frac{\partial V_t}{\partial \eta} + F = 0 \tag{13}$$

where

$$V_t = \frac{2\xi\nu F}{U_e}\frac{\partial \eta}{\partial x} + (2\xi)^{0.5}\frac{V}{U_e}$$

Momentum equation:

$$2\xi F\frac{\partial F}{\partial \xi} + V_t\frac{\partial F}{\partial \eta} = \frac{2\xi(1-F^2)}{U_e}\frac{\partial U_e}{\partial \xi} + \frac{\partial^2 F}{\partial \eta^2} + (2\xi)^{0.5}\frac{\partial S}{\partial \eta} \tag{14}$$

Enthalpy equation:

$$2\xi F\frac{\partial H}{\partial \xi} + V_t\frac{\partial H}{\partial \eta} = -\frac{2\xi FH}{T_e}\frac{\partial T_e}{\partial \xi} + \frac{1}{Pr}\frac{\partial^2 H}{\partial \eta^2} + (2\xi)^{0.5}\frac{\partial \theta}{\partial \eta} \tag{15}$$

Turbulence equations:

$$2\xi F\frac{\partial R_x}{\partial \xi} + V_t\frac{\partial R_x}{\partial \eta} = -2\xi\frac{4R_xF}{U_e}\frac{\partial U_e}{\partial \xi} + \frac{U_e}{\nu}\frac{\partial}{\partial \eta}\left(\Lambda R^{0.5}\frac{\partial R_x}{\partial \eta}\right) + \frac{\partial^2 R_x}{\partial \eta^2} + 2S(2\xi)^{0.5}\frac{\partial F}{\partial \eta} + 2\xi\frac{(R-3R_x)}{3}\frac{\nu R^{0.5}}{\Lambda U_e} + 2\xi R_x\left(-2\frac{\partial F}{\partial \xi} - \frac{2\nu}{U_e}\frac{\partial F}{\partial \eta}\frac{\partial \eta}{\partial x} - \frac{2\nu^2}{U_e^2\Lambda^2}\right) \tag{16}$$

$$2\xi F\frac{\partial R_y}{\partial \xi} + V_t\frac{\partial R_y}{\partial \eta} = 5\frac{U_e}{\nu}\frac{\partial}{\partial \eta}\left(\Lambda R^{0.5}\frac{\partial R_y}{\partial \eta}\right) + \frac{\partial^2 R_y}{\partial \eta^2} + 2\xi\frac{\nu R^{0.5}}{\Lambda U_e}\frac{(R-3R_y)}{3} + 2\xi R_y \times\left(2\frac{\partial F}{\partial \xi} + \frac{2\nu}{U_e}\frac{\partial F}{\partial \eta} + \frac{2\nu}{U_e}\frac{\partial F}{\partial \eta}\frac{\partial \eta}{\partial x} - \frac{2\nu^2}{U_e^2\Lambda^2}\right) \tag{17}$$

$$2\xi F\frac{\partial R_z}{\partial \xi} + V_t\frac{\partial R_z}{\partial \eta} = -2\xi\frac{2R_zF}{U_e}\frac{\partial U_e}{\partial \xi} + \frac{U_e}{\nu}\frac{\partial}{\partial \eta}\left(\Lambda R^{0.5}\frac{\partial R_z}{\partial \eta}\right) + \frac{\partial^2 R_z}{\partial \eta^2} + 2\xi\frac{\nu R^{0.5}}{\Lambda U_e}\frac{(R-3R_z)}{3} - 2\xi R_z\frac{2\nu^2}{U_e^2\Lambda^2} \tag{18}$$

$$2\xi F\frac{\partial S}{\partial u} + V_t\frac{\partial S}{\partial \eta} = -2\xi\frac{2FS}{U_e}\frac{\partial U_e}{\partial \xi} + 3\frac{U_e}{\nu}\frac{\partial}{\partial \eta}\left(\Lambda R^{0.5}\frac{\partial S}{\partial \eta}\right) + \frac{\partial^2 S}{\partial \eta^2} + (2\xi)^{0.5}R_y\frac{\partial F}{\partial \eta} + 2\xi S\left(-\frac{\nu R^{0.5}}{U_e\Lambda} - \frac{2\nu^2}{U_e^2\Lambda^2}\right) \tag{19}$$

and

$$2\xi F\frac{\partial\theta}{\partial\xi}+V_t\frac{\partial\theta}{\partial\eta}=-2\xi\frac{F\theta}{T_e}\frac{\partial T_e}{\partial\xi}+3\frac{U_e}{\nu}\frac{\partial}{\partial\eta}\left(\Lambda R^{0.5}\frac{\partial\theta}{\partial\eta}\right)+\frac{\partial^2\theta}{\partial\eta^2}+(2\xi)^{0.5}R_y\frac{\partial H}{\partial\eta}+2\xi\theta\left(\frac{\partial F}{\partial\xi}+\frac{\nu}{U_e}\frac{\partial F}{\partial\eta}\frac{\partial\eta}{\partial x}-\frac{\nu R^{0.5}}{U_e\Lambda}-\frac{2\nu^2}{U_e^2\Lambda^2}\right) \tag{20}$$

where $R=R_x+R_y+R_z$.

In order to solve the previous governing equations for the mean flow and turbulence properties, the initial and boundary conditions are derived analytically in the following manner.

Initial conditions.—The initial profiles of the mean flow properties and the turbulence correlations at $\varphi=\varphi_0$ are determined analytically from equations (13) to (20). The following assumptions are made:

(1) At η_2 location,

$$\frac{\partial F}{\partial\eta}=0,\quad \frac{\partial H}{\partial\eta}=0$$

$$\frac{\partial R_x}{\partial\eta}=0,\quad \frac{\partial R_y}{\partial\eta}=0,\quad \frac{\partial R_z}{\partial\eta}=0$$

$$\frac{\partial S}{\partial\eta}=0,\quad \frac{\partial\theta}{\partial\eta}=0$$

In addition,

$$F=1,\quad H=1,\quad S=c_5(R_xR_y)^{0.5},\quad \text{and}\quad \theta=0$$

are imposed at η_2. Also, c_5 is an empirical constant; the value $c_5=0.001$ is used in this study.

(2) The Reynolds normal stress components $\overline{u^2}$ and $\overline{v^2}$ are assumed to be independent of φ for very small φ. Therefore, at φ_0,

$$\frac{\partial R_x}{\partial\xi}=R_x\left(\frac{-2}{Re\varphi_0^2}\right) \tag{21}$$

and

$$\frac{\partial R_y}{\partial\xi}=R_y\left(\frac{-2}{Re\varphi_0^2}\right) \tag{22}$$

Similarly,

$$\frac{\partial R_z}{\partial\xi}=R_zf_1(\varphi_0) \tag{23}$$

$$\frac{\partial S}{\partial\xi}=Sf_2(\varphi_0) \tag{24}$$

and

$$\frac{\partial\theta}{\partial\xi}=\theta f_3(\varphi_0) \tag{25}$$

are also assumed at φ_0.

(3) The mean flow is symmetric about the $\varphi=0$ plane. In order to facilitate the analysis, this mean flow behavior is also assumed at small distances away from the stagnation point, $\varphi=0$. Therefore, $\partial F/\partial\xi=0$ and $\partial H/\partial\xi=0$ are imposed along the η direction at the φ_0 location.

(4) The conditions $F=0$, $H=T_w/T_e$, $R_x=0$, $R_y=0$, $R_z=0$, $S=0$, and $\theta=0$ are also imposed at the cylinder surface.

By applying these assumptions (eqs. (21) to (24)) to the turbulence governing equations, the following relations are found at $\varphi=\varphi_0$ and $\eta=\eta_2$:

$$R_{x,o,e}=\frac{\dfrac{\nu R_{o,e}^{1.5}}{3U_{o,e}\Lambda_e}}{\dfrac{-2}{Re\varphi_0^2}+\dfrac{4(dU/d\xi)_{o,e}}{U_{o,e}}+\dfrac{\nu R_{o,e}^{0.5}}{U_{o,e}\Lambda_e}+\dfrac{2\nu^2}{U_{o,e}^2\Lambda_e^2}} \tag{26}$$

$$R_{y,o,e}=\frac{\dfrac{\nu R_{o,e}^{1.5}}{3U_{o,e}\Lambda_e}}{\dfrac{-2}{Re\varphi_0^2}+\dfrac{\nu R_{o,e}^{0.5}}{U_{o,e}\Lambda_e}+\dfrac{2\nu^2}{U_{o,e}^2\Lambda_e^2}} \tag{27}$$

$$f_1(\varphi_0)=-\frac{2(dU/d\xi)_{o,e}}{U_{o,e}}+\frac{\nu R_{o,e}^{1.5}}{3U_{o,e}R_{z,o,e}\Lambda_e} \tag{28}$$

and

$$f_2(\varphi_0)=-\frac{2(dU/d\xi)_{o,e}}{U_{o,e}}-\frac{\nu R_{o,e}^{0.5}}{U_{o,e}\Lambda_e}-\frac{2\nu^2}{U_{o,e}^2\Lambda_e^2} \tag{29}$$

where $R_{o,e}=2\nu aK_2/U_{o,e}^2$ is assumed. Since $\theta=0$ is imposed at η_2, $d\theta/d\xi=0$ occurs at the boundary layer edge. This zero

gradient condition is also used within the boundary layer at $\varphi = \varphi_0$. It follows from the assumption (eq. (25)) that

$$f_3(\varphi_0) = 0 \tag{30}$$

With the aid of $f_1(\varphi_0)$, $f_2(\varphi_0)$, and $f_3(\varphi_0)$, assumption 2 defines the mean flow, streamwise turbulence gradient terms. Substituting the mean flow, streamwise gradients into equations (13) to (20) results in a set of ordinary differential equations with the boundary conditions specified at $\eta = 0$ and $\eta = \eta_2$. These equations are solved numerically for the boundary layer flow property profiles at $\varphi_0 = 0.04°$ in order to avoid the singularity at the stagnation point ($\varphi = 0°$). These property profiles are used as the initial conditions for the downstream, boundary layer flow-field analysis.

Boundary conditions.—The turbulence double correlations along the boundary layer edge are also required to analyze the flow field. The turbulence kinetic energy is first defined by using the k–ϵ two-equation turbulence modeling. The turbulence kinetic energy is then substituted into the Reynolds stress equations to determine the turbulence double correlations.

By following the k–ϵ two-equation turbulence modeling technique (appendix A), the turbulence modeling equations can be written in the x–y coordinate system as

$$ax\frac{dk}{dx} = 4a^2c_\mu\frac{k^2}{\epsilon} - \epsilon + \frac{d}{dx}\left(c_\mu\frac{k^2}{c_{3\epsilon}}\frac{dk}{dx}\right) \tag{31}$$

$$ax\frac{d\epsilon}{dx} = 4a^2c_1c_\mu k - c_2\frac{\epsilon^2}{k} + \frac{d}{dx}\left(c_\mu\frac{k^2}{c_{4\epsilon}}\frac{d\epsilon}{dx}\right) \tag{32}$$

If the coordinate transformations (eq. (1)) and the following forms of solutions for k and ϵ

$$k = \nu aK(\xi) \quad \text{and} \quad \epsilon = \nu a^2E(\xi) \tag{33}$$

are introduced into equations (31) and (32), the turbulence modeling equations become

$$2\xi\frac{dK}{d\xi} = 4c_\mu\frac{K^2}{E} - E + 2\xi\frac{d}{d\xi}\left(c_\mu\frac{K^2}{c_3E}\frac{dK}{d\xi}\right) \tag{34}$$

$$2\xi\frac{dE}{d\xi} = 4c_1c_\mu K - c_2\frac{E^2}{K} + 2\xi\frac{d}{d\xi}\left(c_\mu\frac{K^2}{c_4E}\frac{dE}{d\xi}\right) \tag{35}$$

The analysis of the turbulence in flow region 2 defines the following initial conditions:

$$K = K_2 \quad \text{and} \quad E = E_2 \tag{36}$$

at $\xi = \xi_2$ and $\eta = \eta_2$.

With the assumptions that the gradients $\partial R_x/\partial\eta$, $\partial R_y/\partial\eta$, and $\partial R_z/\partial\eta$ vanish at the boundary layer edge, equations (16), (17), and (18) give the following theoretical relations among the mean velocity, the Reynolds normal stresses, and their mean flow streamwise gradients:

$$\frac{\partial R_{x,e}}{\partial\xi} = -\frac{4R_{x,e}}{U_e}\frac{dU_e}{d\xi} + \frac{\nu}{U_e}\frac{R_e^{1.5}}{3\Lambda_e} - \frac{\nu R_e^{0.5}R_{x,e}}{U_e\Lambda_e} - \frac{2\nu^2}{U_e^2\Lambda_e^2}R_{x,e} \tag{37}$$

$$\frac{\partial R_{y,e}}{\partial\xi} = -\frac{\nu R_e^{1.5}}{3U_e\Lambda_e} - \frac{\nu}{U_e}\frac{R_e^{0.5}R_{y,e}}{\Lambda_e} - \frac{2\nu^2}{U_e^2\Lambda_e^2}R_{y,e} \tag{38}$$

and

$$\frac{\partial R_{z,e}}{\partial\xi} = -\frac{2R_{z,e}}{U_e}\frac{dU_e}{d\xi} + \frac{\nu R_e^{1.5}}{3U_e\Lambda_e} - \frac{\nu R_e^{0.5}}{U_e\Lambda_e}R_{z,e} - \frac{2\nu^2}{U_e^2\Lambda_e^2}R_{z,e} \tag{39}$$

The previous equations can be solved for the Reynolds normal stresses. The sum of the Reynolds normal stresses R should be consistent with the turbulence kinetic energy obtained from equations (34) and (35). The Reynolds normal stresses along the boundary layer edge are determined from this consistency requirement. Therefore, the following analysis is used.

The previous analysis of the initial profiles defines the Reynolds normal stresses at $\xi = \xi_2$ and $\eta = \eta_2$. These are the initial conditions to integrate equations (37) to (39) along the downstream direction. In this study, the fourth-order Runge-Kutta numerical method is used. The turbulence kinetic energy obtained previously from equations (34) and (35) is used to evaluate the derivatives. The integration step is adjusted until the turbulence kinetic energy $(R_{x,e} + R_{y,e} + R_{z,e})U_e^2/2$ satisfactorily converges to the corresponding value predicted by the k–ϵ two-equation turbulence modeling. The corresponding Reynolds normal stresses are the boundary conditions at the boundary layer edge.

Finally, the following conditions are also imposed:

(1) At the boundary layer edge $\eta = \eta_2$, $F_e = 1$, $H_e = 1$, $S_e = c_5(R_{x,e}R_{y,e})^{0.5}$, and $\theta = 0$.

(2) At the surface $\eta = 0$, $F = 0$, $H = T_w/T_e$, $R_x = 0$, $R_y = 0$, $R_z = 0$, $S = 0$, and $\theta = 0$.

A numerical computational procedure to calculate the boundary layer flow field was developed in a previous study (ref. 18). This numerical method and the other computational procedures used in this study are described in appendix C.

Results and Comparison with Experiment

In order to verify the previous theoretical analysis, a numerical computation was performed to predict the existing measurements. A set of detailed experimental data on the effect of free-stream turbulence on heat transfer from heated cylinders placed normal to the airstream was reported by Lowery and Vachon (ref. 5). Tests were conducted over a range of Reynolds numbers and at different turbulence levels. The two-point turbulence longitudinal correlations in the free stream were measured. These data can be used to determine the turbulence longitudinal microlength scale that is required to start the present numerical calculations. Thus, the test conditions of this reference experiment were used as input to the present numerical computational procedures.

Examples of the free-stream turbulence longitudinal correlation and the corresponding turbulence longitudinal microlength scales, with $Tu = 0.013$, 0.017, and 0.028, and $Re = 2.50\times10^5$, are shown in figure 2. The microlength scales were obtained by curve-fitting the experimental data with equation (3). On the basis of the free-stream mean velocity, the free-stream turbulence intensity, and the turbulence longitudinal microlength scale, the present numerical computational procedures were performed to calculate the turbulence kinetic energy, the turbulence double correlations, and the mean flow properties within the stagnation flow field. The surface heat transfer rate was also calculated from the mean temperature distribution. In the following sections, these numerical results are described and are compared with the experiment of reference 5.

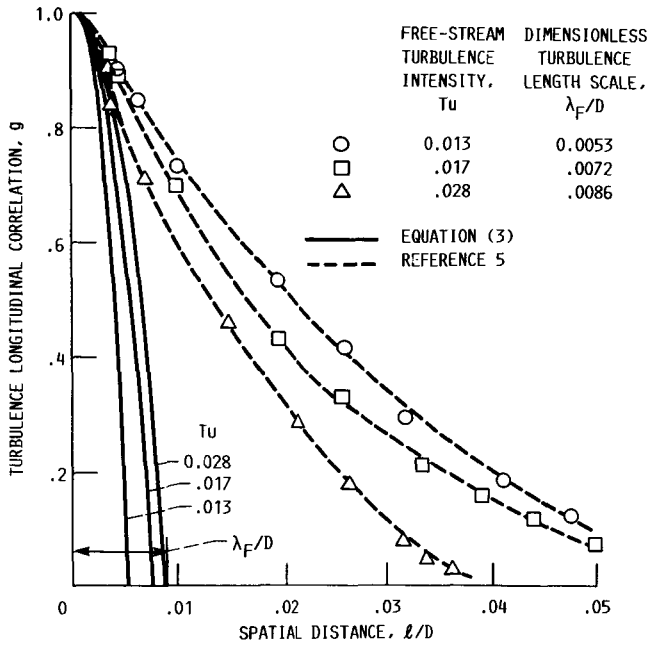

Figure 2.—Free-stream turbulence longitudinal microlength scale. Reynolds number Re, 2.50×10^5.

Turbulence

To show the variation of the turbulence kinetic energy along the stagnation-point streamline, some analytical results are plotted in figure 3. Except for the lowest turbulence case, the turbulence kinetic energy increased within the inviscid flow region in the direction toward the surface and reached a maximum value at the boundary layer edge. The turbulence kinetic energy then decreased continuously and vanished at the cylinder surface. This turbulence kinetic energy variation is similar to the result in reference 13. However, the present analysis predicts a reduction in the turbulence kinetic energy along the stagnation-point streamline when the free-stream turbulence intensity and Reynolds number are small ($Tu = 0.013$ and $Re = 1.90\times10^5$).

Examples of the Reynolds normal stress profiles within the boundary layer at the stagnation point are shown in figure 4. These results are for the cases with $Re = 2.50\times10^5$ and $Tu = 0.017$ and 0.028. The Reynolds normal stresses decreased continuously from the boundary layer edge in a direction normal to the surface. Large values of R_y among the Reynolds normal stresses were calculated within a small region near the surface. These Reynolds normal stress profiles differed significantly from those of a flat-plate turbulent boundary layer (ref. 20), where the largest Reynolds normal stress was measured in the x direction.

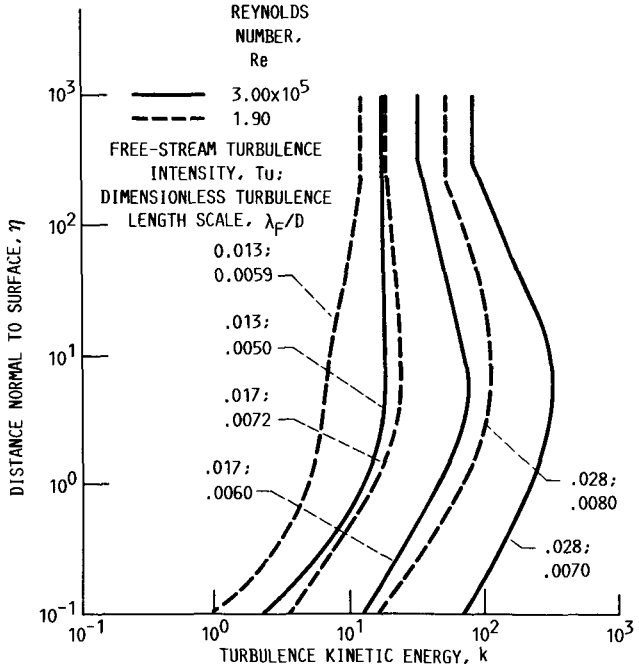

Figure 3.—Turbulence kinetic energy along stagnation streamline.

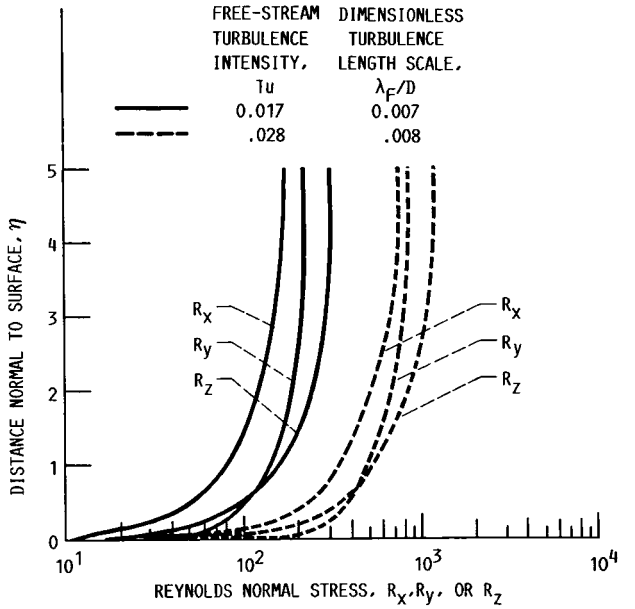

Figure 4.—Reynolds normal stress profiles within stagnation-point boundary layer. Reynolds number Re, 2.50×10^5.

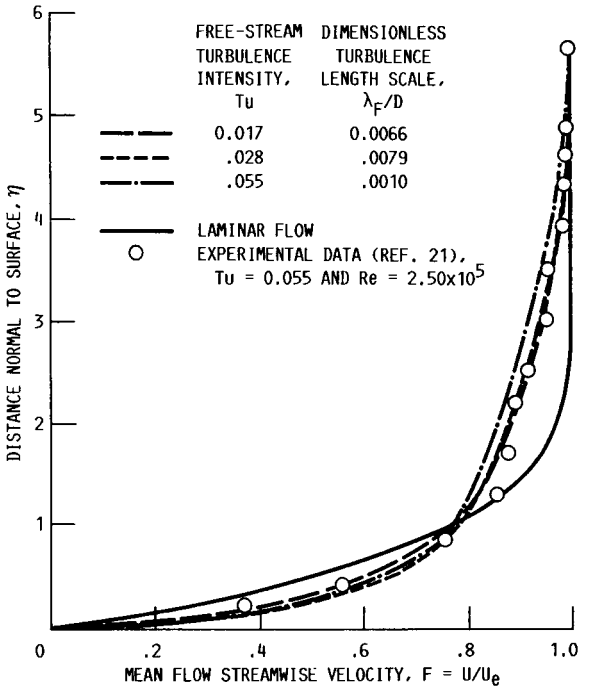

Figure 5.—Mean flow streamwise velocity component within stagnation-point boundary layer. Reynolds number Re, 2.50×10^5.

The analytical predictions of the mean velocity component, $F = U/U_e$, within the boundary layer at $\varphi = \varphi_0$ are shown in figure 5. These profiles are compared with the mean velocity profile of the theoretical laminar boundary layer. The comparison shows that the free-stream turbulence increased the velocity near the surface and decreased the velocity near the boundary layer edge. Existing measurements (ref. 21) of this velocity component with $Re = 2.50\times10^5$ and $Tu \approx 0.05$ are also plotted in this figure. The analytical results are in good agreement with the measurements.

Examples of the computational results of the turbulence kinetic energy and the Reynolds normal stresses along the boundary layer edge are shown in figure 6. In this figure, the turbulence properties are nondimensionalized with the corresponding stagnation-point values. The turbulence kinetic energy increased continuously along the downstream direction. The rate of change in the kinetic energy is a function of the free-stream turbulence properties λ_F, Tu, and Re. A large increase in the turbulence kinetic energy was found for the case with small free-stream turbulence intensity and a small Reynolds number. The Reynolds normal stress components $\overline{u_e^2}$ and $\overline{v_e^2}$ increased at the downstream locations. However, the $\overline{w_e^2}$ component was reduced near the stagnation point. The effect of the microlength scale on the Reynolds normal stress along the boundary layer edge is shown in figure 7. The computational results for the cases with $Re = 2.50\times10^5$ and $Tu = 0.028$ but different length scales, $\lambda_F/D = 0.0053$ and 0.0079, are presented. The turbulence microlength scale affected the Reynolds stress distributions. Increasing the length scale decreased the ratio of $\overline{u_e^2}/\overline{u_{o,e}^2}$ and increased the ratio of $\overline{w_e^2}/\overline{w_{o,e}^2}$ along the boundary layer edge. No significant difference in the ratio of $\overline{v_e^2}/\overline{v_{o,e}^2}$ was calculated.

Surface Heat Transfer

The present analytical results of the surface heat transfer are defined in terms of the Nusselt number

$$Nu = \frac{-D\left(\dfrac{\partial T}{\partial y}\right)_{y=0}}{T_w - T_F} \tag{40}$$

The mean temperature gradient $(\partial T/\partial y)_{y=0}$ at the surface was calculated numerically from the mean temperature profile, which in turn, was obtained previously from the solution of the boundary layer flow.

The analytical results for the stagnation-point surface heat transfer rate over a range of the free-stream Reynolds number and the turbulence intensity are compared with the experimental data (ref. 5) and existing correlations (refs. 5 and 6) in figure 8. The surface heat transfer rate is expressed in the form of the Froessling number ($Nu\ Re^{-0.5}$). Linear variation in the turbulence longitudinal microlength scale as a function of the free-stream Reynolds number was also assumed in the present calculation. The turbulence longitudinal microlength scale decreased as the Reynolds number increased. With constant free-stream turbulence intensity, turbulence microlength scales within ±10 percent of the values in figure 2 were used in the numerical computation for a range of the free-

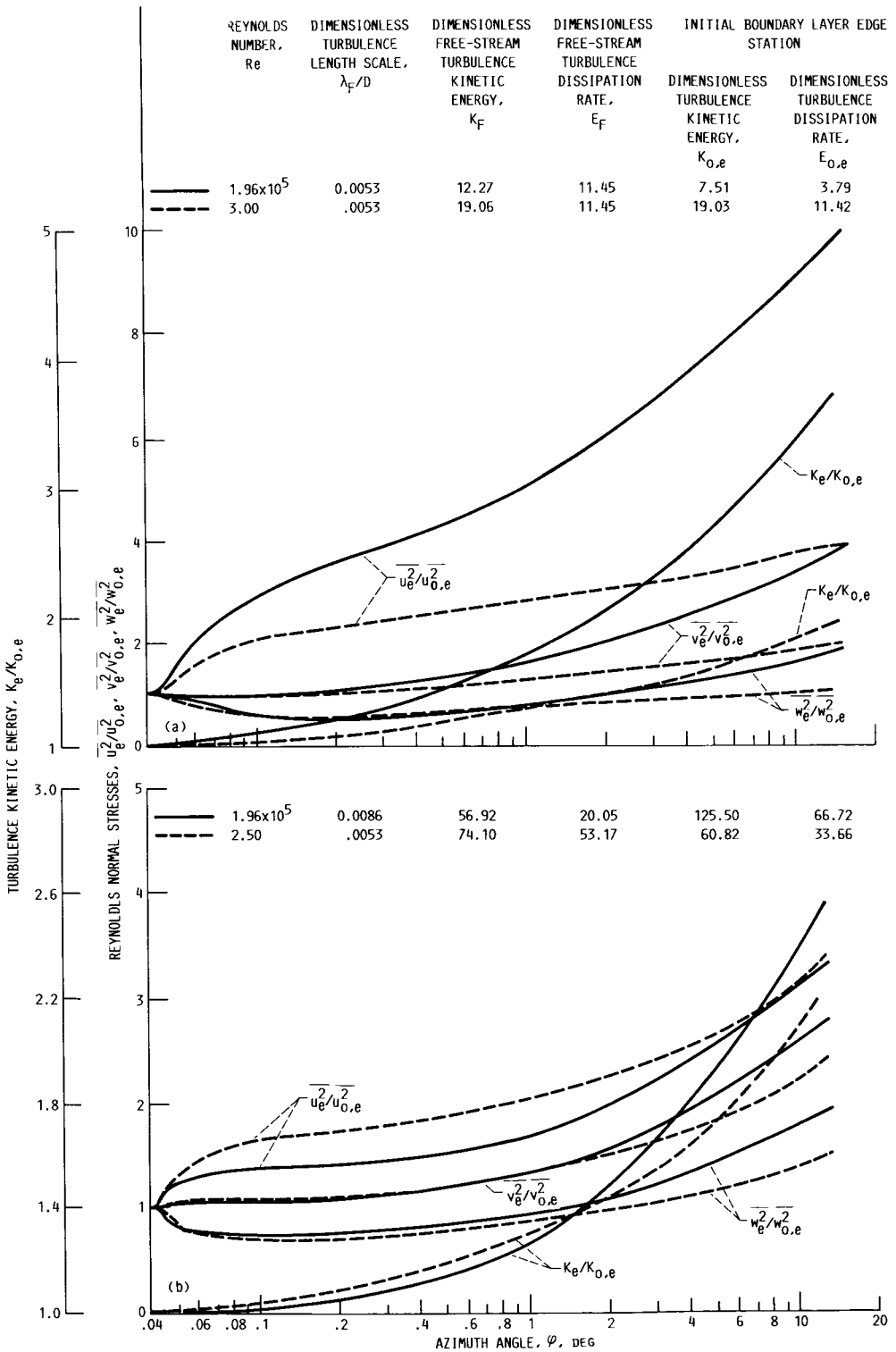

(a) Turbulence intensity *Tu*, 0.013.
(b) Turbulence intensity *Tu*, 0.028.

Figure 6.—Turbulence kinetic energy and Reynolds normal stresses along boundary layer edge.

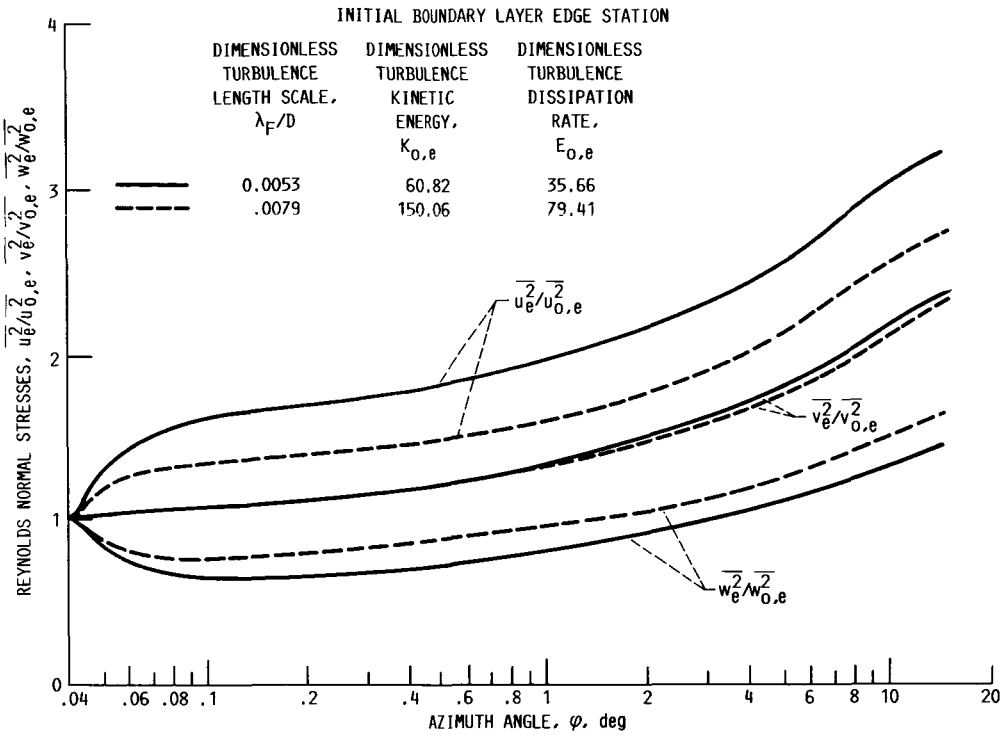

Figure 7.—Effect of turbulence longitudinal microlength scale on Reynolds normal stresses along boundary layer edge. Reynolds number Re, 2.50×10^5; free-stream turbulence intensity Tu, 0.028.

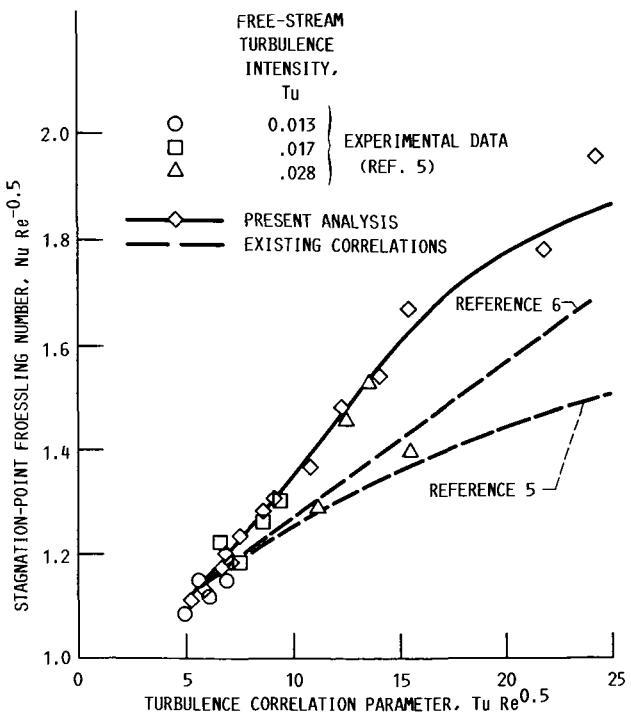

Figure 8.—Comparison of stagnation-point Froessling number between analysis and experimental correlations.

stream Reynolds number of $1.50 \le Re\times10^{-5} \le 3.00$. Because it includes the effect of the free-stream turbulence microlength scale, the present analysis calculates a larger stagnation-point surface heat transfer rate than is indicated by the correlations in references 5 and 6.

Examples of the computational results of the turbulence double correlation $-\overline{vt}/U_eT_e$ within the boundary layer at the stagnation point are shown in figure 9. The maximum turbulence correlation occurs near the surface. Increasing the free-stream turbulence intensity also increases the turbulence correlation $\overline{vt}$. Together with the characteristics of the Reynolds normal stress component (fig. 4), the present analysis indicates that the free-stream turbulence penetrates into the near-surface flow region and induces a large turbulence correlation $\overline{vt}$. Thus, a surface heat transfer rate larger than that for laminar flow occurs.

Some analytical results of the surface heat transfer rate within a small distance from the stagnation point are plotted in figure 10 in terms of the Froessling number. An approximately constant Froessling number is calculated only for the case with $Tu = 0.013$. For $Tu = 0.017$ and 0.028, the analytical results show a reduction in the Froessling number near the stagnation point. With high free-stream turbulence intensity, a large turbulence dissipation rate may occur near the stagnation point. This turbulence dissipation rate reduces the rate of the increase in the turbulence kinetic energy. This rate of increase in K_e is not enough to induce a constant surface heat transfer rate.

To investigate the effect of the turbulence longitudinal microlength scale on the surface heat transfer rate, we

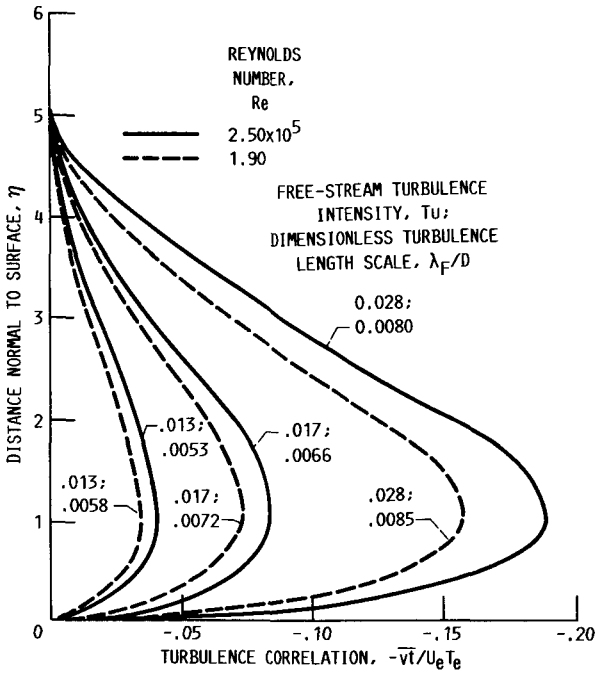

Figure 9.—Profiles of turbulence correlation $\overline{vt}$ within stagnation-point boundary layer.

compared the analytical results of the turbulence kinetic energy and the Froessling number for $\lambda_F/D = 0.0053$ and 0.0079 with $Re = 2.50\times10^5$ and $Tu = 0.028$ in figure 11. With $\lambda_F/D = 0.0079$, the present analysis computed the experimental data in reference 5. A lower level of the turbulence kinetic energy and a smaller Froessling number were also predicted for the case with a small free-stream turbulence longitudinal microlength scale. These computational results also show a reduction in the Froessling number near the stagnation point.

In this study, the approximation

$$S_e = c_5(R_{x,e}R_{y,e})^{0.5}$$

was used along the boundary layer edge. This approximation is similar to the correlation observed from the flat-plate turbulent boundary layer study (ref. 20). In the present analysis, $c_5 = 0.001$ was found to give the best computational results. In an earlier study (ref. 18), a different value of c_5 (0.0001) was used because the boundary layer edge location and the corresponding turbulence kinetic energy (or the Reynolds normal stresses) were not analyzed theoretically. If one uses the smaller value of c_5, then a small (nonzero) $\overline{uv}$ is imposed along the boundary layer edge. This approximation is different from the k–ϵ two-equation turbulence modeling, which requires $S_e = 0$ for the external flow field in this study. However, the requirement of $S_e = 0$ is itself an assumption.

The assumption $\overline{vt}_e = 0$ was also imposed at the boundary layer edge. Intuitively, the turbulence dynamic equations can

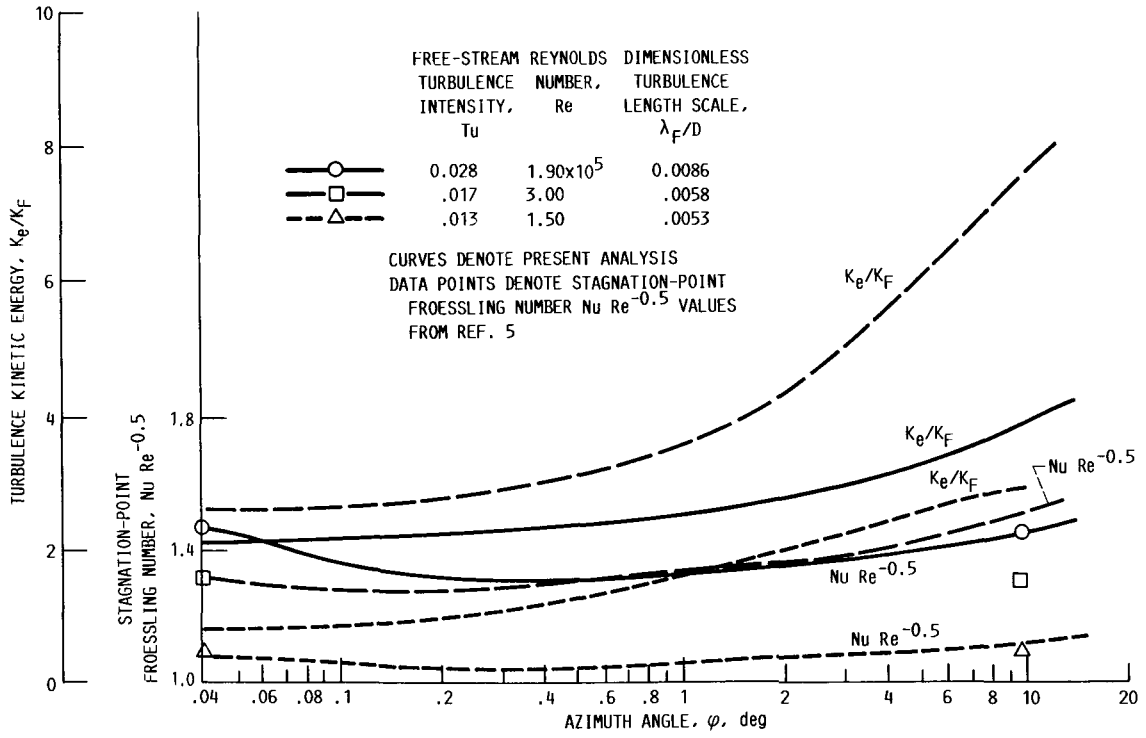

Figure 10.—Boundary layer edge turbulence kinetic energy and corresponding Froessling number.

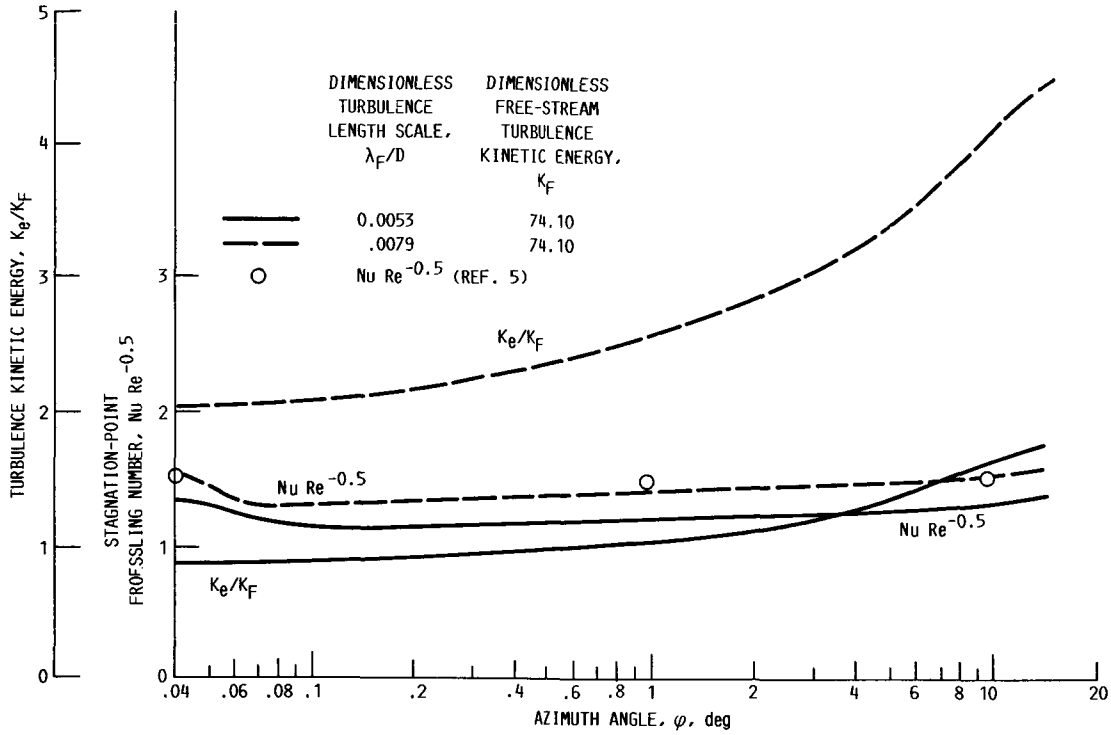

Figure 11.—Effect of turbulence longitudinal microlength scale on turbulence kinetic energy at boundary layer edge and Froessling number. Reynolds number *Re*, 2.50×10^5; turbulence intensity *Tu*, 0.028.

also be used to study the variation of the turbulence double correlation $\overline{vt}$ within the external flow region. If $\overline{vt}$ is nonzero in the external flow field, then a different $\overline{vt}$ distribution may occur within the boundary layer flow region, and the present analysis will predict different stagnation-flow surface heat transfer rates. If this is true, it might resolve the different levels of the stagnation-flow surface heat transfer rate reported in various experiments. Although the task requires the $\overline{vt}$ boundary condition within the free stream, the effect of the free-stream temperature fluctuation on the surface heat transfer rate of the stagnation flow can be studied by using the present analysis.

Conclusions

A theoretical analysis was formulated to model the effect of the free-stream turbulence on the surface heat transfer of a stagnation-flow region. The flow field of interest was around the forward stagnation point of a circular cylinder in a turbulent flow. The k–ϵ two-equation turbulence modeling was used to analyze the turbulence kinetic energy within the external inviscid flow region. The time-averaged turbulence transport equations were employed to predict the turbulence double correlations within the boundary layer. From the boundary layer edge conditions of the turbulence kinetic energy, the transport equations of the mean flow and turbulence were solved numerically for the turbulence double correlations, the mean velocity, and the mean temperature.

The present analytical results show that, depending on the free-stream turbulence properties, different levels of turbulence kinetic energy occur along the boundary layer edge. These different levels of turbulence kinetic energy induce different surface heat transfer rates. Increasing the free-stream turbulence intensity or the turbulence longitudinal microlength scale also increases the stagnation-region surface heat transfer rate. It is postulated that the free-stream turbulence penetrates into the boundary layer and induces high surface heat transfer rates.

The analysis presents a procedure to calculate the stagnation-point surface heat transfer rate as a function of the free-stream turbulence intensity, the turbulence longitudinal microlength scale, and the Reynolds number. Because of limited data on the turbulence longitudinal microlength scale, this analysis was verified only for some cases with a Reynolds number of the order of 10^5 and a free-stream turbulence intensity of less than 5 percent. By considering the free-stream turbulence longitudinal microlength scale, this analysis predicts a higher stagnation-point surface heat transfer rate than was obtained from the existing correlations relating the free-stream turbulence intensity, the Reynolds number, and the surface heat transfer rate.

Lewis Research Center
National Aeronautics and Space Administration
Cleveland, Ohio, June 2, 1987

Appendix A
k–ϵ Two-Equation Turbulence Modeling

Launder and Spalding (ref. 22) developed the k–ϵ two-equation turbulence modeling technique. It has been found effective by many researchers in modeling the turbulence of different turbulent flow configurations. In the present study, this technique is also used to model the turbulence along the stagnation-point streamline and the boundary layer edge.

k–ϵ Transport Equations

With a two-dimensional mean flow field, the modeling equations for the turbulence kinetic energy k and the turbulence dissipation rate ϵ can be written in an x–y orthogonal coordinate system as

$$U\frac{\partial k}{\partial x}+V\frac{\partial k}{\partial y}=\frac{\partial}{\partial x}\left(\frac{\nu_t}{c_3}\frac{\partial k}{\partial x}\right)+\frac{\partial}{\partial y}\left(\frac{\nu_t}{c_3}\frac{\partial k}{\partial y}\right)-\overline{u^2}\frac{\partial U}{\partial x}-\overline{uv}\left(\frac{\partial V}{\partial x}+\frac{\partial U}{\partial y}\right)-\overline{v^2}\frac{\partial V}{\partial y}-\epsilon \tag{A1}$$

and

$$U\frac{\partial \epsilon}{\partial x}+V\frac{\partial \epsilon}{\partial y}=\frac{\partial}{\partial x}\left(\frac{\nu_t}{c_4}\frac{\partial \epsilon}{\partial x}\right)+\frac{\partial}{\partial y}\left(\frac{\nu_t}{c_4}\frac{\partial \epsilon}{\partial y}\right)-c_1\frac{\epsilon}{k}\overline{u^2}\frac{\partial U}{\partial x}-c_1\frac{\epsilon}{k}\overline{uv}\left(\frac{\partial V}{\partial x}+\frac{\partial U}{\partial y}\right)-c_1\frac{\epsilon}{k}\overline{v^2}\frac{\partial V}{\partial y}-c_2\frac{\epsilon^2}{k} \tag{A2}$$

The turbulent dynamic viscosity ν_t is related to k and ϵ by $\nu_t = c_\mu k^2/\epsilon$. The closure assumptions for the Reynolds stresses are

$$\left.\begin{aligned}-\overline{u^2}&=2\nu_t\frac{\partial U}{\partial x}-\frac{2}{3}k\\-\overline{uv}&=\nu_t\left(\frac{\partial U}{\partial y}+\frac{\partial V}{\partial x}\right)\\-\overline{v^2}&=2\nu_t\frac{\partial V}{\partial y}-\frac{2}{3}k\end{aligned}\right\} \tag{A3}$$

and c_1, c_2, c_3, c_4, and c_μ are empirical constants. The following values are usually used in the turbulence flow analysis: $c_1 = 1.44$, $c_2 = 1.92$, $c_3 = 1.00$, $c_4 = 1.30$, and $c_\mu = 0.09$.

Applications of k–ϵ Equations

The k and ϵ equations are used to predict the turbulence kinetic energy along the stagnation-point streamline in flow region 2 and the boundary layer edge between flow regions 2 and 3. The mathematical formulations of the k and ϵ equations are described in the following section.

Along Stagnation-Point Streamline

The turbulence kinetic energy variation along the stagnation-point streamline is analyzed. For the stagnation-point flow field, the inviscid flow analysis predicts the mean flow velocity components as

$$U = ax \quad \text{and} \quad V = -ay \tag{A4}$$

with $a = 4V_F/D$. Therefore, the velocity gradients

$$\frac{\partial U}{\partial x}=a,\quad \frac{\partial U}{\partial y}=0,\quad \frac{\partial V}{\partial x}=0,\quad \frac{\partial V}{\partial y}=-a \tag{A5}$$

are found from equation (A4).

Substituting the previous relations into equations (A1) and (A2) results in these equations being simplified and becoming

$$ay\frac{dk}{dy}=-4a^2c_\mu\frac{k^2}{\epsilon}+\epsilon-\frac{d}{dy}\left(c_\mu\frac{k^2}{c_{3\epsilon}}\frac{dk}{dy}\right) \tag{A6}$$

$$ay\frac{d\epsilon}{dy}=-4a^2c_1c_\mu k+c_2\frac{\epsilon^2}{k}-\frac{d}{dy}\left(c_\mu\frac{k^2}{c_{4\epsilon}}\frac{d\epsilon}{dy}\right) \tag{A7}$$

Furthermore, by introducing the coordinate transformations (eq. (1)) into the previous equations, the k–ϵ two-equation turbulence modeling becomes

$$a\eta\frac{dk}{d\eta}=-4a^2c_\mu\frac{k^2}{\epsilon}+\epsilon-\frac{a}{\nu}\frac{d}{d\eta}\left(c_\mu\frac{k^2}{c_{3\epsilon}}\frac{dk}{d\eta}\right) \tag{A8}$$

$$a\eta\frac{d\epsilon}{d\eta}=-4a^2c_1c_\mu k+c_2\frac{\epsilon^2}{k}-\frac{a}{\nu}\frac{d}{d\eta}\left(c_\mu\frac{k^2}{c_{4\epsilon}}\frac{d\epsilon}{d\eta}\right) \tag{A9}$$

We are seeking the solutions of k and ϵ in the forms

$$k = \nu a K(\eta) \quad \text{and} \quad \epsilon = \nu a^2 E(\eta) \tag{A10}$$

Substituting the previous definitions into equations (A8) and (A9) results in the following dimensionless turbulence modeling equations being obtained along the stagnation-point streamline:

$$\eta \frac{dK}{d\eta} = -4c_\mu \frac{K^2}{E} + E - \frac{d}{d\eta}\left(c_\mu \frac{K^2}{c_3 E}\frac{dK}{d\eta}\right) \tag{A11}$$

$$\eta \frac{dE}{d\eta} = -4c_1 c_\mu K + c_2 \frac{E^2}{K} - \frac{d}{d\eta}\left(c_\mu \frac{K^2}{c_4 E}\frac{dE}{d\eta}\right) \tag{A12}$$

Along Boundary Layer Edge

Equations (A1) and (A2) are also used to analyze the turbulence kinetic energy along the boundary layer edge. The basic assumptions are that the gradients $\partial k/\partial y$ and $\partial \epsilon/\partial y$ vanish at the boundary layer edge. Thus, the k and ϵ equations become

$$U\frac{\partial k}{\partial x} = c_\mu \frac{k^2}{\epsilon} 2\left(\frac{\partial U}{\partial x}\right)^2 + 2\left(\frac{\partial V}{\partial y}\right)^2 + \left(\frac{\partial U}{\partial y} + \frac{\partial V}{\partial x}\right)^2 - \epsilon + \frac{\partial}{\partial x}\left(c_\mu \frac{k^2}{c_3 \epsilon}\frac{\partial k}{\partial x}\right) \tag{A13}$$

$$U\frac{\partial \epsilon}{\partial x} = c_1 c_\mu k\left[2\left(\frac{\partial U}{\partial x}\right)^2 + 2\left(\frac{\partial V}{\partial y}\right)^2 + \left(\frac{\partial U}{\partial y} + \frac{\partial V}{\partial x}\right)^2\right] - c_2 \frac{\epsilon^2}{k} + \frac{\partial}{\partial x}\left(c_\mu \frac{k^2}{c_4 \epsilon}\frac{\partial \epsilon}{\partial x}\right) \tag{A14}$$

The closure assumptions (eqs. (A3)) are also used in deriving the previous k and ϵ equations. The mean velocity properties in equations (A13) and (A14) are substituted with the results in equations (A4) and (A5). The k and ϵ equations become

$$ax\frac{dk}{dx} = 4a^2 c_\mu \frac{k^2}{\epsilon} - \epsilon + \frac{d}{dx}\left(c_\mu \frac{k^2}{c_3 \epsilon}\frac{dk}{dx}\right) \tag{A15}$$

$$ax\frac{d\epsilon}{dx} = 4a^2 c_1 c_\mu k - c_2 \frac{\epsilon^2}{k} + \frac{d}{dx}\left(c_\mu \frac{k^2}{c_4 \epsilon}\frac{d\epsilon}{dx}\right) \tag{A16}$$

Again, the x coordinate is transformed by using equation (1). The following forms of solutions for k and ϵ are also sought:

$$k(\xi) = \nu a K(\xi) \quad \text{and} \quad \epsilon(\xi) = \nu a^2 E(\xi) \tag{A17}$$

Paralleling the results in flow region 2, the following dimensionless forms of the k and ϵ equations are obtained through mathematical manipulations:

$$2\xi\frac{dK}{d\xi} = 4c_\mu \frac{K^2}{E} - E + 2\xi\frac{d}{d\xi}\left(c_\mu \frac{K^2}{c_3 E}\frac{dK}{d\xi}\right) \tag{A18}$$

$$2\xi\frac{dE}{d\xi} = 4c_1 c_\mu K - c_2 \frac{E^2}{K} + 2\xi\frac{d}{d\xi}\left(c_\mu \frac{K^2}{c_4 E}\frac{dE}{d\xi}\right) \tag{A19}$$

Appendix B
Turbulence Transport Equations

For engineering applications, the concepts of eddy viscosity and eddy conductivity have been used by researchers to calculate the momentum and heat transfer in turbulent flow. However, in cases where the dynamics of turbulence is important, the concept of eddy transport may not be sufficient to study the turbulence. Thus, Donaldson et al. (refs. 16 and 17) developed a method, the method of invariant modeling, to model the dynamics of the turbulence correlations. It is used in this study to analyze the turbulence within the boundary layer flow region.

Turbulence Transport Equations

The one-point turbulence dynamic equations are used in the method of invariant modeling. The details in reference 16 are followed to derive the transport equations for the turbulence double correlations $\overline{u^2}$, $\overline{v^2}$, $\overline{w^2}$, $\overline{uv}$, and $\overline{vt}$ in the x-y-z coordinate system. These equations are

$$U\frac{\partial \overline{u^2}}{\partial x} + V\frac{\partial \overline{u^2}}{\partial y} = -2\,\overline{uv}\frac{\partial U}{\partial y} - 2\,\overline{u^2}\frac{\partial U}{\partial x} + \frac{2}{\rho}\overline{p\frac{\partial u}{\partial x}} - \frac{\partial}{\partial y}\overline{vuu} + \nu\frac{\partial^2 \overline{u^2}}{\partial y^2} - 2\nu\overline{\frac{\partial u}{\partial x_i}\frac{\partial u}{\partial x_i}} \tag{B1}$$

$$U\frac{\partial \overline{v^2}}{\partial x} + V\frac{\partial \overline{v^2}}{\partial y} = 2\,\overline{v^2}\frac{\partial U}{\partial x} + \frac{2}{\rho}\overline{p\frac{\partial v}{\partial y}} - \frac{\partial}{\partial y}\overline{vvv} + \frac{2}{\rho}\frac{\partial}{\partial y}\overline{vp} + \nu\frac{\partial^2 \overline{v^2}}{\partial y^2} - 2\nu\overline{\frac{\partial v}{\partial x_i}\frac{\partial v}{\partial x_i}} \tag{B2}$$

$$U\frac{\partial}{\partial x}\overline{w^2} + V\frac{\partial}{\partial y}\overline{w^2} = \frac{2}{\rho}\overline{p\frac{\partial w}{\partial z}} - \frac{\partial}{\partial y}\overline{vww} + \nu\frac{\partial^2 \overline{w^2}}{\partial y^2} - 2\nu\overline{\frac{\partial w}{\partial x_i}\frac{\partial w}{\partial x_i}} \tag{B3}$$

$$U\frac{\partial}{\partial x}\overline{uv} + V\frac{\partial}{\partial y}\overline{uv} = -\overline{v^2}\frac{\partial U}{\partial y} + \frac{1}{\rho}\overline{p\left(\frac{\partial v}{\partial y} + \frac{\partial v}{\partial x}\right)} - \frac{\partial}{\partial y}\overline{vuv} + \frac{1}{\rho}\frac{\partial}{\partial y}\overline{pu} + \nu\frac{\partial^2}{\partial y^2}\overline{uv} - 2\nu\overline{\frac{\partial u}{\partial x_i}\frac{\partial v}{\partial x_i}} \tag{B4}$$

and

$$U\frac{\partial}{\partial x}\overline{vt} + V\frac{\partial}{\partial y}\overline{vt} = -\overline{v^2}\frac{\partial T}{\partial y} + \overline{vt}\frac{\partial U}{\partial x} - \frac{1}{\rho}\frac{\partial}{\partial y}\overline{pt} + \frac{1}{\rho}\overline{p\frac{\partial t}{\partial y}} - \frac{\partial}{\partial y}\overline{vvt} + \nu\frac{\partial^2}{\partial y^2}\overline{vt} - 2\nu\overline{\frac{\partial v}{\partial x_i}\frac{\partial t}{\partial x_i}} \tag{B5}$$

Turbulence Closure Assumptions

Assumptions for the higher-order turbulence correlation terms in equations (B1) to (B5) must be made so that these turbulence equations and the mean flow transport equations can form a closed system of equations to describe the flow field. These closure assumptions are based on the turbulence double correlations and a length scale Λ. In this study, the following forms of the closure assumptions (refs. 16 and 17) are used:

$$\frac{2}{\rho}\overline{p\frac{\partial u}{\partial x}} = \frac{1}{\rho}\left[\frac{\rho\left(\overline{u^2}+\overline{v^2}+\overline{w^2}\right)^{0.5}}{\Lambda}\right]\left[\frac{\overline{u^2}+\overline{v^2}+\overline{w^2}}{3} - \overline{u^2}\right]$$

$$\frac{2}{\rho}\overline{p\frac{\partial v}{\partial y}} = \frac{1}{\rho}\left[\frac{\rho\left(\overline{u^2}+\overline{v^2}+\overline{w^2}\right)^{0.5}}{\Lambda}\right]\left[\frac{\overline{u^2}+\overline{v^2}+\overline{w^2}}{3} - \overline{v^2}\right]$$

$$\frac{2}{\rho}\overline{p\frac{\partial w}{\partial z}} = \frac{1}{\rho}\left[\frac{\rho\left(\overline{u^2}+\overline{v^2}+\overline{w^2}\right)^{0.5}}{\Lambda}\right]\left[\frac{\overline{u^2}+\overline{v^2}+\overline{w^2}}{3} - \overline{w^2}\right]$$

$$\frac{1}{\rho}\overline{p\left(\frac{\partial u}{\partial y} + \frac{\partial v}{\partial x}\right)} = \frac{1}{\rho}\left[\frac{\rho\left(\overline{u^2}+\overline{v^2}+\overline{w^2}\right)^{0.5}}{\Lambda}\right]\left(-\overline{uv}\right)$$

$$\frac{1}{\rho}\overline{p\frac{\partial t}{\partial y}} = \frac{1}{\rho}\left[\frac{\rho\left(\overline{u^2}+\overline{v^2}+\overline{w^2}\right)^{0.5}}{\Lambda}\right]\left(-\overline{vt}\right)$$

$$\frac{1}{\rho}\frac{\partial}{\partial y}\overline{vp} = -\frac{1}{\rho}\frac{\partial}{\partial y}\left[\rho\Lambda\left(\overline{u^2}+\overline{v^2}+\overline{w^2}\right)^{0.5}\frac{\partial \overline{u^2}}{\partial y}\right]$$

$$\frac{1}{\rho}\frac{\partial}{\partial y}\overline{up} = -\frac{1}{\rho}\frac{\partial}{\partial y}\left[\rho\Lambda\left(\overline{u^2}+\overline{v^2}+\overline{w^2}\right)^{0.5}\frac{\partial\overline{uv}}{\partial y}\right]$$

$$\frac{1}{\rho}\frac{\partial}{\partial y}\overline{pt} = -\frac{1}{\rho}\frac{\partial}{\partial y}\left[\rho\Lambda\left(\overline{u^2}+\overline{v^2}+\overline{w^2}\right)^{0.5}\frac{\partial\overline{vt}}{\partial y}\right]$$

$$\frac{\partial}{\partial y}\overline{vuu} = -\frac{\partial}{\partial y}\left[\Lambda\left(\overline{u^2}+\overline{v^2}+\overline{w^2}\right)^{0.5}\frac{\partial\overline{u^2}}{\partial y}\right]$$

$$\frac{\partial}{\partial y}\overline{vvv} = -\frac{\partial}{\partial y}\left[3\Lambda\left(\overline{u^2}+\overline{v^2}+\overline{w^2}\right)^{0.5}\frac{\partial\overline{v^2}}{\partial y}\right]$$

$$\frac{\partial}{\partial y}\overline{vww} = -\frac{\partial}{\partial y}\left[\Lambda\left(\overline{u^2}+\overline{v^2}+\overline{w^2}\right)^{0.5}\frac{\partial\overline{w^2}}{\partial y}\right]$$

$$\frac{\partial}{\partial y}\overline{vuv} = -\frac{\partial}{\partial y}\left[2\Lambda\left(\overline{u^2}+\overline{v^2}+\overline{w^2}\right)^{0.5}\frac{\partial\overline{uv}}{\partial y}\right]$$

$$\frac{\partial}{\partial y}\overline{vvt} = -\frac{\partial}{\partial y}\left[2\Lambda\left(\overline{u^2}+\overline{v^2}+\overline{w^2}\right)^{0.5}\frac{\partial}{\partial y}\overline{vt}\right]$$

$$\nu\,\overline{\frac{\partial u}{\partial x_i}\frac{\partial u}{\partial x_i}} = \nu\frac{\overline{u^2}}{\Lambda^2}, \qquad \nu\,\overline{\frac{\partial v}{\partial x_i}\frac{\partial v}{\partial x_i}} = \nu\frac{\overline{v^2}}{\Lambda^2}$$

$$\nu\,\overline{\frac{\partial w}{\partial x_i}\frac{\partial w}{\partial x_i}} = \nu\frac{\overline{w^2}}{\Lambda^2}, \qquad \nu\,\overline{\frac{\partial u}{\partial x_i}\frac{\partial v}{\partial x_i}} = \nu\frac{\overline{uv}}{\Lambda^2}$$

and

$$\nu\,\overline{\frac{\partial v}{\partial x_i}\frac{\partial t}{\partial x_i}} = \nu\frac{\overline{vt}}{\Lambda^2}$$

The length scale distribution within the boundary layer in flow region 3 of this study is also assumed to be similar to the mixing length profile of a flat-plate turbulent boundary layer. Within a small distance from the surface, the length scale varies linearly as a function of the normal distance from the surface. Away from the surface, the length scale remains constant. This length scale profile is shown schematically in figure 12. The pivot point location y_p is equal to 10 percent of the theoretical laminar stagnation-point boundary layer thickness δ. At the boundary layer edge, we found that the length scale Λ_e can be related to the free-stream turbulence intensity by

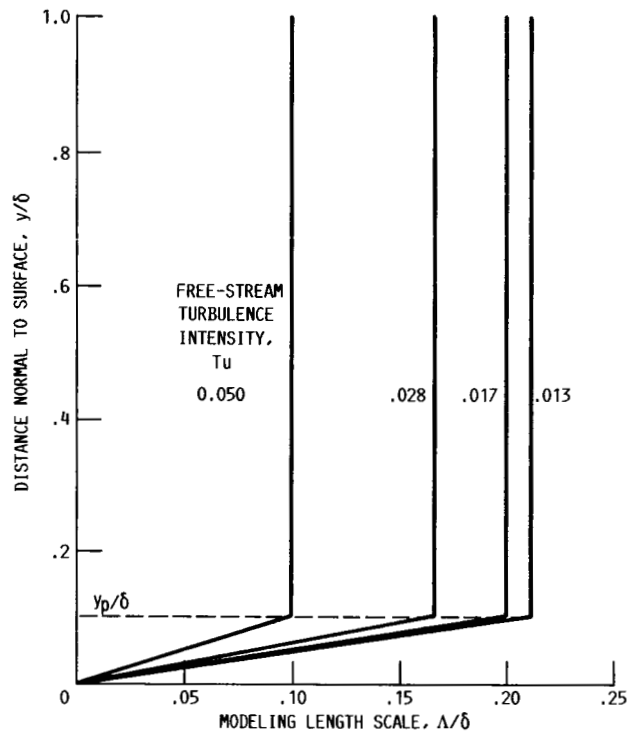

Figure 12.—Modeling length scale of turbulence closure assumption.

$$\Lambda_e = (0.25 - 3Tu)\delta \tag{B6}$$

Applications of Turbulence Transport Equations

In the present study, the mean flow is two dimensional, steady, and incompressible. It is described by the following turbulent boundary layer continuity, momentum, and enthalpy equations:

$$\frac{\partial U}{\partial x} + \frac{\partial V}{\partial y} = 0 \tag{B7}$$

$$U\frac{\partial U}{\partial x} + V\frac{\partial U}{\partial y} = -\frac{1}{\rho}\frac{\partial P}{\partial x} + \frac{\partial}{\partial y}\left(\nu\frac{\partial U}{\partial y} - \overline{uv}\right) \tag{B8}$$

$$U\frac{\partial T}{\partial x} + V\frac{\partial T}{\partial y} = \frac{\partial}{\partial y}\left(\frac{\kappa}{\rho c_p}\frac{\partial T}{\partial y} - \overline{vt}\right) \tag{B9}$$

The turbulence double correlations $\overline{uv}$ and $\overline{vt}$ are modeled by using the turbulence dynamic equations. They are obtained by substituting the turbulence closure assumptions into equations (B1) to (B5). Thereby, the turbulence dynamic equations are found to be

$$U\frac{\partial\overline{u^2}}{\partial x}+V\frac{\partial\overline{u^2}}{\partial y}=-2\overline{uv}\frac{\partial U}{\partial y}-2\,\overline{u^2}\frac{\partial U}{\partial x}+\frac{\left(u^2+v^2+w^2\right)^{0.5}}{\Lambda}\left(\frac{\overline{v^2}+\overline{w^2}-2\overline{u^2}}{3}\right)+\frac{\partial}{\partial y}\left[\Lambda\left(\overline{u^2}+\overline{v^2}+\overline{w^2}\right)^{0.5}\frac{\partial\overline{U^2}}{\partial y}\right]+\nu\frac{\partial^2\overline{u^2}}{\partial y^2}-2\nu\frac{\overline{u^2}}{\Lambda^2} \tag{B10}$$

$$U\frac{\partial\overline{v^2}}{\partial x}+V\frac{\partial\overline{v^2}}{\partial y}=-2\overline{v^2}\frac{\partial U}{\partial x}+\frac{\left(\overline{u^2}+\overline{v^2}+\overline{w^2}\right)^{0.5}}{\Lambda}\left(\frac{\overline{u^2}+\overline{w^2}-2\overline{v^2}}{3}\right)+5\frac{\partial}{\partial y}\left[\Lambda\left(\overline{u^2}+\overline{v^2}+\overline{w^2}\right)^{0.5}\frac{\partial\overline{v^2}}{\partial y}\right]+\nu\frac{\partial^2\overline{v^2}}{\partial y^2}-2\nu\frac{\overline{v^2}}{\Lambda^2} \tag{B11}$$

$$U\frac{\partial\overline{w^2}}{\partial x}+V\frac{\partial\overline{w^2}}{\partial y}=\frac{\left(\overline{u^2}+\overline{v^2}+\overline{w^2}\right)^{0.5}}{\Lambda}\left(\frac{\overline{u^2}+\overline{v^2}-2\overline{w^2}}{3}\right)+\frac{\partial}{\partial y}\left[\Lambda\left(\overline{u^2}+\overline{v^2}+\overline{w^2}\right)^{0.5}\frac{\partial\overline{w^2}}{\partial y}\right]+\nu\frac{\partial^2\overline{w^2}}{\partial y^2}-2\nu\frac{\overline{w^2}}{\Lambda^2} \tag{B12}$$

$$U\frac{\partial\overline{uv}}{\partial x}+V\frac{\partial\overline{uv}}{\partial y}=-\overline{v^2}\frac{\partial U}{\partial y}+\frac{\left(\overline{u^2}+\overline{v^2}+\overline{w^2}\right)^{0.5}}{\Lambda}\overline{uv}-\frac{\left(\overline{u^2}+\overline{v^2}+\overline{w^2}\right)^{1.5}}{3\Lambda}-3\frac{\partial}{\partial y}\left[\Lambda\left(\overline{u^2}+\overline{v^2}+\overline{w^2}\right)^{0.5}\frac{\partial\overline{uv}}{\partial y}\right]-\nu\frac{\partial^2\overline{uv}}{\partial y^2}+2\nu\frac{\overline{uv}}{\Lambda^2} \tag{B13}$$

and

$$U\frac{\partial\overline{vt}}{\partial x}+V\frac{\partial\overline{vt}}{\partial y}=-\overline{v^2}\frac{\partial T}{\partial y}-\overline{vt}\frac{\partial U}{\partial x}+\frac{\left(\overline{u^2}+\overline{v^2}+\overline{w^2}\right)^{0.5}}{\Lambda}\times\overline{vt}-3\frac{\partial}{\partial y}\left[\Lambda\left(\overline{u^2}+\overline{v^2}+\overline{w^2}\right)^{0.5}\frac{\partial\overline{vt}}{\partial y}\right]-\nu\frac{\partial^2\overline{vt}}{\partial y^2}+\frac{2\nu\overline{vt}}{\Lambda^2} \tag{B14}$$

Together with the length scale assumptions, the previous equations form a closed system of turbulence transport equations. These equations are used to analyze the turbulence and the mean flow properties in the boundary layer flow region. They are nondimensionalized according to the procedures in reference 23. The resulting dimensionless equations were reported in a previous study (ref. 18).

Appendix C
Numerical Computation

The finite difference method is used to calculate the turbulence and the mean flow properties within the flow field. Summaries of the finite difference scheme and the numerical computational procedures are presented in this appendix.

Finite Difference Scheme

All of the transport equations (eqs. (A11), (A12), (A18), (A19), and (14) to (20)) can be represented by the following equation:

$$A_{G1}\frac{\partial G}{\partial \eta} + A_{G2}\frac{\partial G}{\partial \eta} = A_{G3}G + A_{G4}\frac{\partial}{\partial \eta}\left(A_{G5}\frac{\partial G}{\partial \eta}\right) + A_{G6}\frac{\partial}{\partial \eta}\left(A_{G7}\frac{\partial G}{\partial \eta}\right) + A_{G8}\frac{\partial^2 G}{\partial \eta^2} + A_{G9} \tag{C1}$$

where G is either a turbulence or a mean flow property. A comparison between equation (C1) and each transport equation shows that A_{Gi} (i = 1 to 9) may be constant, or the functions of the properties and their gradients, or the coordinates ξ and η. The transport equations are written in the forms of equation (C1) to describe the finite difference scheme.

k–ϵ Turbulence Modeling Equations

In flow region 2, either of the dimensionless equations (A11) and (A12) can be written as

$$A_{G2}\frac{\partial G}{\partial \eta} = A_{G3}G + A_{G6}\frac{\partial}{\partial \eta}\left(A_{G7}\frac{\partial G}{\partial \eta}\right) + A_{G9} \tag{C2}$$

with $G = K$ or E.

Similarly, equations (A18) and (A19) in flow region 3 can also be written as

$$A_{G1}\frac{\partial G}{\partial \xi} = A_{G3}G + A_{G4}\frac{\partial}{\partial \xi}\left(A_{G5}\frac{\partial G}{\partial \xi}\right) + A_{G9} \tag{C3}$$

with $G = K$ or E.

Equation (C3) has a form similar to equation (C2) regardless of the difference between the ξ and η coordinates. A similar finite difference scheme is used to convert equations (C2) and (C3) into finite difference forms. As an illustration, the steps in transforming equation (C2) are described in the following paragraphs.

The following central finite difference scheme with variable grid size in the η direction is used. The derivatives at each grid point m are approximated by

$$\left(\frac{\partial G}{\partial \eta}\right)_m = \frac{G_{m+1} - G_{m-1}}{\eta_{m+1} - \eta_{m-1}} \tag{C4}$$

and

$$\left[\frac{\partial\left(A_{G7}\dfrac{\partial G}{\partial \eta}\right)}{\partial \eta}\right]_m = \frac{2A_{G7,m+1/2}}{(\eta_{m+1} - \eta_m)(\eta_{m+1} - \eta_{m-1})}G_{m+1} - \left[\frac{2A_{G7,m+1/2}}{(\eta_{m+1} - \eta_m)(\eta_{m+1} - \eta_{m-1})} + \frac{2A_{G7,m-1/2}}{(\eta_m - \eta_{m-1})(\eta_{m+1} - \eta_{m-1})}\right]G_m + \frac{2A_{G7,m-1/2}}{(\eta_{m+1} - \eta_{m-1})(\eta_m - \eta_{m-1})}G_{m-1} \tag{C5}$$

where

$$A_{G7,m+1/2} = \frac{(A_{G7,m+1} + A_{G7,m})}{2}$$

$$A_{G7,m-1/2} = \frac{(A_{G7,m} + A_{G7,m-1})}{2}$$

Substituting the previous expressions into equation (C2) yields a finite difference equation,

$$B_1 G_{m+1} + B_2 G_m + B_3 G_{m-1} = B_4 \tag{C6}$$

at each grid point m. The coefficients B_i (i = 1 to 4) are functions of the various coefficients A_{Gi} and the grid size at the grid points $m + 1$, m, and $m - 1$.

Applying the previous mathematical manipulation at every grid point within the interval $\eta_1 \geq \eta \geq \eta_2$ results in a set of finite difference equations for equation (C2). The boundary conditions of G are specified at η_1 and η_2. This set of equations is solved for the G values at each grid point m.

Boundary Layer Flow Transport Equations

All of the governing equations (eqs. (14) to (20)) can be written in the following form:

$$A_{G1}\frac{\partial G}{\partial \xi} + A_{G2}\frac{\partial G}{\partial \eta} = A_{G3}G + A_{G6}\frac{\partial}{\partial \eta}\left(A_{G7}\frac{\partial G}{\partial \eta}\right) + A_{G8}\frac{\partial^2 G}{\partial \eta^2} + A_{G9} \tag{C7}$$

where G can be one of the mean flow properties or the turbulence double correlations.

For the initial profile calculation, the assumptions and the results in the initial profile analysis are used to define $\partial G/\partial \xi$. For the downstream calculations, the gradient $\partial G/\partial \xi$ is approximated by

$$\left(\frac{\partial G}{\partial \xi}\right)_m = \frac{(G_m - G_m^P)}{\Delta \xi} \tag{C8}$$

where G_m^P is the G_m at the previous station. Constant grid size is used in the η direction. The derivatives in the η direction are approximated with the following central finite difference scheme:

$$\left(\frac{\partial G}{\partial \eta}\right)_m = \frac{G_{m+1} - G_{m-1}}{2\Delta \eta} \tag{C9}$$

$$\left(\frac{\partial^2 G}{\partial \eta^2}\right)_m = \frac{G_{m+1} - 2G_m + G_{m-1}}{(\Delta \eta)^2} \tag{C10}$$

and

$$\left[\frac{\partial\left(A_{G7}\dfrac{\partial G}{\partial \eta}\right)}{\partial \eta}\right]_m = \frac{[A_{G7,m+1/2}G_{m+1} - (A_{G7,m+1/2} + A_{G7,m-1/2})G_m + A_{G7,m-1/2}G_{m-1}]}{(\Delta \eta)^2} \tag{C11}$$

with

$$A_{G7,m+1/2} = \frac{A_{G7,m+1} + A_{G7,m}}{2}$$

$$A_{G7,m-1/2} = \frac{A_{G7,m} + A_{G7,m-1}}{2}$$

Substituting the previous relations into equation (C7) produces a set of finite difference equations, similar to the form of equation (C6), for each of the governing equations (eqs. (14) to (20)).

Computational Procedure

The sets of finite difference equations are solved by using iterative numerical procedures. Depending on the boundary conditions, slightly different iterative schemes are employed in the numerical computations.

k–ϵ Turbulence Modeling Equations

Different procedures are used in flow regions 2 and 3. They are described separately in the following sections.

Flow region 2.—Equations (10) to (12) describe the boundary condition at $\eta = \eta_1$ and η_2. However, η_2 is not defined. Therefore, η_2 is first assigned an arbitrary value to start the numerical calculation. The existing analysis (ref. 13) indicates that η_2 is approximately 5. Linear variations in K and E are first assumed. The coefficients of the finite difference equations are evaluated with these K and E assumptions. Thus, two sets of linear algebraic equations are obtained to relate K and E at the grid point locations. Since K and E are prescribed at η_1 and η_2, these equations are solved for K and E distributions by using the method of successive substitution.

The previous procedures are repeated until K and E converge at each grid point. The boundary values of K and E at η_2 are adjusted to ensure that the K and E profiles satisfy the boundary conditions (eqs. (11) and (12)).

The convergence in K and E is sensitive to their assumed values at the start of the computations. On the basis of k–ϵ two-equation turbulence modeling, Strahle (ref. 15) developed analytical links between the turbulence properties k and ϵ at the stagnation point and in the free stream. By neglecting the diffusion terms and using the same value for the empirical constants c_1 and c_2 (i.e., $c_1 = c_2 = 1.90$), these analytical links can be written as

$$k_2 = \left(\frac{2.4V_F}{D\epsilon_F}\right)^{1.111} k_F^{2.111} \tag{C12}$$

and

$$\epsilon_2 = \left(\frac{2.4V_F k_F}{D}\right)^{2.111} \epsilon_F^{-1.111} \tag{C13}$$

According to equation (7), the previous relations are nondimensionalized and they become

$$K_2 = \left(\frac{0.6}{E_F}\right)^{1.111} K_F^{2.111} \tag{C14}$$

and

$$E_2 = (0.6K_F)^{2.111} E_F^{-1.111} \tag{C15}$$

With the isotropic assumptions (eq. (2)) in flow region 1, the approximate boundary conditions for K and E at η_2 are calculated from the previous relations. These K and E values are used to start the numerical computations.

The grid size within the computational interval is generated by using the model in reference 23. Three hundred to four hundred grid points are used in the computations. The grid is tightened near η_1 and η_2 to ensure the boundary conditions.

Flow region 3.—The aforementioned numerical calculation provides the conditions of K and E at ξ_2. From these conditions, the K and E along the boundary layer edge are also calculated by using the sets of finite difference equations corresponding to equations (34) and (35). The computational domain $\xi_2 \leq \xi \leq \xi_3$ is limited to a small region near the stagnation point. In this study, ξ_3, corresponding to $\varphi = 15°$, was chosen.

The numerical procedure is similar to that used in flow region 2. First, K and E at the ξ_3 location are estimated and linear distributions in K and E between ξ_2 and ξ_3 are assumed. The coefficients of the finite difference equations are calculated by using the assumed K and E distributions. Two sets of linear algebraic equations, relating the K and E at the grid points, are obtained. These algebraic equations are solved with the method of successive substitution to update the K and E distributions. This iterative computational procedure is repeated until K and E converge at each grid point. The numerical values of K and E at ξ_3 are also adjusted in each iteration to facilitate the convergence in the numerical computations.

The grid size within the computational interval is also generated with the technique used in flow region 2. Two hundred to three hundred grid points are used in the present computations. The grid is also tightened near ξ_2 and ξ_3.

Boundary Layer Flow Equations

The numerical computational procedure was developed previously in reference 18. It contains two main routines at each ξ downstream location. First, the velocity field is calculated. This velocity field is then substituted into the energy equation to compute the temperature distributions.

Similar routines are repeated at the next downstream locations. At each ξ station, the property G at the previous ξ station is used to define the coefficients A_{Gi} in the first iteration, and the updated value for G at the current station is then used to determine these coefficients in the next iteration. However, in the initial profile calculations, the coefficients A_{Gi} are calculated by using the laminar stagnation-point boundary layer flow profiles.

For the cases calculated in this study, the computational domain is limited to $0.04° \leq \varphi \leq 15°$ and $\eta \leq 6.0$. Constant grid size ($\Delta\eta = 0.05$) in the η direction and variable step size along the ξ direction ($\Delta\xi$ corresponding to $\Delta\varphi = 0.01°$ for $\varphi \leq 0.2°$ and $\Delta\varphi = 0.2°$ for $\varphi \geq 0.2°$) are used.

References

1. Zapp, G.M., Jr.: The Effect of Turbulence on Local Heat Transfer Coefficients Around a Cylinder Normal to an Airstream. MS Thesis, Oregon State College, 1950.
2. Schnautz, J.A.: Effect of Turbulence Intensity on Mass Transfer from Plates, Cylinders, and Spheres in Air Streams. Ph.D. Thesis, Oregon State University, 1958.
3. Seban, R.A.: The Influence of Free Stream Turbulence on the Local Heat Transfer from Cylinders. J. Heat Trans., vol. 82, no. 2, May 1960, pp. 101-107.
4. Kestin, J.; Maeder, P.F.; and Sogin, H.H.: The Influence of Turbulence on the Transfer of Heat to Cylinders near the Stagnation Point. Z. Angew. Math. Phys., vol. 12, no. 2, 1961, pp. 115-132.
5. Lowery, G.W.; and Vachon, R.I.: The Effect of Turbulence on Heat Transfer from Heated Cylinders. Int. J. Heat Mass Trans., vol. 18, no. 11, Nov. 1975, pp. 1229-1242.
6. Smith, M.C.; and Kuethe, A.M.: Effects of Turbulence on Laminar Skin Friction and Heat Transfer. Phys. Fluids, vol. 9, no. 12, Dec. 1966, pp. 2337-2344.
7. Gorla, R.S.R.: Combined Influence of Unsteady Free Stream Velocity and Free Stream Turbulence on Stagnation Point Heat Transfer. 1983 Tokyo International Gas Turbine Congress, vol. 1, Gas Turbine Society of Japan, Tokyo, 1984, pp. 45-49. (Also, ASME Paper 83-GTJ-17, Oct. 1983.)
8. Kestin, J.; and Wood, R.T.: The Influence of Turbulence on Mass Transfer from Cylinders. J. Heat Trans., vol. 93, no. 4, Nov. 1971, pp. 321-327.
9. Sutera, S.P.; Maeder, P.F.; and Kestin, J.: On the Sensitivity of Heat Transfer in the Stagnation-Point Boundary Layer to Free-Stream Vorticity. J. Fluid Mech., vol. 16, pt. 4, Aug. 1963, pp. 497-520.
10. Sutera, S.P.: Vorticity Amplification in Stagnation-Point Flow and Its Effect on Heat Transfer. J. Fluid Mech., vol. 21, pt. 3, Mar. 1965, pp. 513-534.
11. VanFossen, G.J.; and Simoneau, R.J.: Preliminary Results of a Study of the Relationship Between Free Stream Turbulence and Stagnation Region Heat Transfer. ASME Paper 85-GT-84, Mar. 1985. (Also, NASA TM-86884.)
12. Hijikata, H.; Yoshida, H.; and Mori, Y.: Theoretical and Experimental Study of Turbulence Effects on Heat Transfer Around the Stagnation Point of a Cylinder. Heat Transfer 1982, vol. 3, U. Grigull, et al., eds., Hemisphere Publishing Corp., 1982, pp. 165-170.
13. Traci, R.M.; and Wilcox, D.C.: Freestream Turbulence Effects on Stagnation Point Heat Transfer. AIAA J., vol. 13, no. 7, July 1975, pp. 890-896.
14. Saffman, P.G.; and Wilcox, D.C.: Turbulence-Model Predictions for Turbulent Boundary Layers. AIAA J., vol. 12, no. 4, Apr. 1974, pp. 541-546.
15. Strahle, W.C.: Stagnation Point Flows with Freestream Turbulence—The Matching Condition. AIAA J., vol. 23, no. 11, Nov. 1985, pp. 1822-1824.
16. Donaldson, C.duP.; Sullivan, R.D.; and Rosenbaum, H.: A Theoretical Study of the Generation of Atmospheric-Clear Air Turbulence. AIAA J., vol. 10, no. 2, Feb. 1972, pp. 162-170.
17. Donaldson, C.duP.: A Computer Study of an Analytical Model of Boundary-Layer Transition. AIAA J., vol. 7, no. 2, Feb. 1969, pp. 271-278.
18. Wang, C.R.: Turbulence and Surface Heat Transfer Near the Stagnation Point of a Circular Cylinder in Turbulent Flow. ASME Paper 84-WA/HT-73, Dec. 1984. (Also, NASA TM-83732.)
19. Hinze, J.O.: Turbulence, McGraw-Hill, New York, 1959.
20. Schlichting, H.: Boundary Layer Theory, 4th ed., McGraw-Hill, New York, 1960.
21. Kestin, J.; and Richardson, P.D.: The Effects of Free-Stream Turbulence and of Sound Upon Heat Transfer. ARL 69-0062, Wright-Patterson AFB, Dayton, OH., Apr. 1969.
22. Launder, B.E.; and Spalding, D.B.: The Numerical Computation of Turbulent Flows. Comput. Methods Appl. Mech. Eng., vol. 3, no. 2, Mar. 1974, pp. 269-289.
23. Beckwith, I.E.; and Bushnell, D.M.: Detailed Description and Results of a Method for Computing Mean and Fluctuating Quantities in Turbulent Boundary Layers. NASA TN D-4815, 1968.
24. Andre, P.; Creff, R.; and Batina, J.: Numerical Study in Heat Transfer for a Turbulent Pulsed Ducted Flow. Numerical Heat Transfer, vol. 9, no. 2, 1986, pp. 201-216.

NASA
National Aeronautics and Space Administration

Report Documentation Page

1. Report No.	2. Government Accession No.	3. Recipient's Catalog No.
NASA TP-2758		

4. Title and Subtitle	5. Report Date
Application of Turbulence Modeling to Predict Surface Heat Transfer in Stagnation Flow Region of Circular Cylinder	September 1987
	6. Performing Organization Code

7. Author(s)	8. Performing Organization Report No.
Chi R. Wang and Frederick C. Yeh	E-3418
	10. Work Unit No.
	505-62-21

9. Performing Organization Name and Address	11. Contract or Grant No.
National Aeronautics and Space Administration Lewis Research Center Cleveland, Ohio 44135-3191	
	13. Type of Report and Period Covered
12. Sponsoring Agency Name and Address	Technical Paper
National Aeronautics and Space Administration Washington, D.C. 20546-0001	14. Sponsoring Agency Code

15. Supplementary Notes

16. Abstract

A theoretical analysis and numerical calculations for the turbulent flow field and for the effect of free-stream turbulence on the surface heat transfer rate of a stagnation flow are presented. The emphasis is on the modeling of turbulence and its augmentation of surface heat transfer rate. The flow field considered is the region near the forward stagnation point of a circular cylinder in a uniform turbulent mean flow. The free stream is steady and incompressible with a Reynolds number of the order of 10^5 and turbulence intensity of less than 5 percent. For this analysis, the flow field is divided into three regions: (1) a uniform free-stream region where the turbulence is homogeneous and isotropic; (2) an external inviscid flow region where the turbulence is distorted by the variation of the mean flow velocity; and (3) an anisotropic turbulent boundary layer region over the cylinder surface. The turbulence modeling techniques used are the k-ϵ two-equation model in the external flow region and the time-averaged turbulence transport equation in the boundary layer region. The turbulence double correlations, the mean velocity, and the mean temperature within the boundary layer are solved numerically from the transport equations. The surface heat transfer rate is calculated as functions of the free-stream turbulence longitudinal microlength scale, the turbulence intensity, and the Reynolds number. The analytical results are compared with existing experiments.

17. Key Words (Suggested by Author(s))	18. Distribution Statement
Heat transfer Boundary layer Turbulence	Unclassified – Unlimited Subject Category 34

19. Security Classif. (of this report)	20. Security Classif. (of this page)	21. No of pages	22. Price*
Unclassified	Unclassified	22	A02

NASA FORM 1626 OCT 86

*For sale by the National Technical Information Service, Springfield, Virginia 22161

NASA-Langley, 1987